



Mineral Composition and Grain Size Effects on the Fracture and Acoustic Emission (AE) Characteristics of Rocks Under Compressive and Tensile Stress

Kun Du¹ · Yu Sun¹ · Jian Zhou¹ · Manoj Khandelwal² · Fengqiang Gong³

Received: 26 October 2021 / Accepted: 2 June 2022 / Published online: 22 July 2022
© The Author(s) 2022

Abstract

The influence of rock mineral composition and mineral grain size on basic rock strength performance and AE characteristics have been studied, 13 different rocks microstructures are analyzed in an optical microscope thin section using petrographic image analysis, making it possible to determine the mineral composition and mineral texture characteristics of rocks. Then, the basic strength parameters of rock and AE signals generated during fracture propagation were obtained by UCT (uniaxial compression test) and BIT (Brazilian intension test). Finally, the relationship between basic strength parameters and AE characteristics of rock with mineral composition and grain size was analyzed. The results showed that different mineral constituents have significant effects on rock strength. The positive influence of plagioclase content on igneous strength was obtained. Sedimentary rocks strength increases initially and then decreases with the increase of plagioclase content. Besides, with the increase in quartz and K-feldspar content, the strength of the rock was weakened obviously. It is also found that the greater the dimensional deviation of mineral grain, the greater the strength of the rock. The strength of igneous rocks was inversely proportional to the mineral grain size, but there is no correlation between the sedimentary rocks strength and the mineral grain size. Furthermore, the tension–shear crack propagation of rock can effectively distinguish by judging that the data set of the AF–RA density graph was nearby the AF axis or RA axis and the peak frequency data sets of below 100 kHz or more than. Alterations in the rock nature are the main key reasons for the differences between AE hit rate, AE count rate, AE energy, and cumulative energy. The plagioclase content and grain size play a decisive role in AE signal characteristics and failure mode.

Highlights

- The relationship between basic strength parameters (i.e., σ_c , σ_t and E) and AE characteristics of rock with mineral composition and grain size was analyzed with 13 different rocks.
- The positive influence of plagioclase content on igneous strength was obtained. Sedimentary rocks strength increases initially and then decreases with the increasing plagioclase content.
- The strength of igneous rocks was inversely proportional to the mineral grain size, but there is no correlation between the sedimentary rocks strength and the mineral grain size.
- The AF–RA nuclear density map and AE peak frequency can effectively distinguish the shear and tensile failure of rocks
- The plagioclase content and grain size play a decisive role in AE signal characteristics and failure mode.

Keywords Mineral composition · Grain size · Acoustic emission · Mechanical property parameters · Rock static parameters

✉ Jian Zhou
j.zhou@csu.edu.cn

✉ Manoj Khandelwal
m.khandelwal@federation.edu.au

² Institute of Innovation, Science and Sustainability, Federation University Australia, Ballarat, VIC 3350, Australia

³ School of Civil Engineering, Southeast University, Nanjing 211189, China

¹ School of Resources and Safety Engineering, Central South University, Changsha 410083, Hunan, China

1 Introduction

The mechanical properties of natural rocks are the result of multiple factors, such as mineral composition, texture characteristics (grain size, grain shape, and arrangement), weathering, porosity, etc. (Ozcelik et al. 2013; Ulusay et al. 1994; Irfan 1996; Du et al. 2020c, 2021; Wang et al. 2020; Tuğrul and Zarif, 1999; Dunn et al. 1973; Ozcelik et al. 2013; KH 1974; Wong et al. 1996). The uniaxial compressive strength (σ_c), tensile strength (σ_t), and elasticity (E) as three commonly used parameters to reflect the differences among different rock types (Torabi-Kaveh et al. 2015; Du et al. 2019, 2022; Zhou et al. 2022a, 2022b; Tao et al. 2021). A number of scholars have studied the effects of rock mineral composition (Tuğrul and Zarif 1999; Richard et al. 1970; Hecht et al. 2005; Gunsallus et al. 1984), grain size, and shape (Tuğrul and Zarif 1999; Wong et al. 1996; Brace 1961; Onodera and Asoka Kumara 1980; Přikryl 2001; Olsson 1974; Handin et al. 1957), weathering (Irfan 1996; Irfan and Dearman 1978; Gupta and Rao 2000), porosity (Dunn et al. 1973; Ozcelik et al. 2013; Li and Dearman 2003; Baud et al. 2014), on the basic strength parameters of specific rocks. In general, the rocks may be classified into three categories: igneous, metamorphic, and sedimentary.

It is well known that mineral grain size as one of the most important factors in rock mechanical properties should be taken into consideration for investigating the mechanical behavior of rocks. Handin et al. studied fine and coarse limestone and found that the fine-grain limestone is generally harder than the coarse-grain limestone, and the σ_c of the fine-grain limestone is higher than the coarse grain limestone (Handin et al. 1957). Wong et al. studied marble, a metamorphic rock, and found that the σ_c of marble decreases with an increase of the reciprocal of the square root of the average grain size (Wong et al. 1996). Similar conclusions were also obtained using some magmatic crystalline rocks by Olsson (1974) and Onodera and Asoka Kumara (1980). Furthermore, Přikryl (2001) proposed an exponential relationship between granites' σ_c and grain size. He found that σ_c of granites increases with the finer grain size of rock-forming minerals. Lindqvist et al. concluded that σ_c of rocks were higher with complex grain shapes and grain geometry boundary of rocks (Lindqvist et al. 2007). Based on the previous experimental results, it can be said that the strength of rocks has a positive relation with complex grain shape and grain geometry boundary but negative relation with the mineral grain size. Furthermore, rocks strength also has a close correlation with the minerals composition. The quartz content is mostly discussed while analyzing the mineral content effects on the strength characteristics of rocks. Richard found that the tensile strength of California granite was inversely proportional to quartz content, and this phenomenon was attributed to

structural differences (Richard et al. 1970). For California granite, the quartz content had a strong positive correlation with uniaxial compressive strength (Gunsallus et al. 1984). However, for different lithological rocks, the quartz content has little correlation with the σ_c (Shakoor and Bonelli 1991). Tuğrul and Zarif concluded that K-feldspar has a weakening effect on the rocks compressive strength (Tuğrul and Zarif 1999). Li et al. studied the effect of porosity on rock strength and concluded that as the porosity increases, the mechanical parameters of rocks decrease (Li and Dearman 2003). Weathering effect is also strongly similar to the porosity effect. Gupta and Rao (2000) found that with the increase in weathering degree, the rock strength decreased, and the failure mode was also affected by the degree of weathering.

Acoustic emission (AE), an engineering technique to monitor the production of rock fissures and cracks has been widely used in mechanical experiments (Khandelwal and Ranjith 2017; Zhen et al. 2021; Novikov et al. 2018; Dong et al. 2021; Xue et al. 2021; Liu et al. 2021; Rui et al. 2022). Recently, Du et al. connected the AE signals released from rock crack propagation with the failure mode of rocks and found that the distribution of AE density maps and AE frequency can effectively distinguish the failure mode of rocks (Du et al. 2016, 2020a, b). In addition, the minerals grain size and composition influence on AE characteristics has also been prevalently researched by analyzing the AE parameter value or distribution, i.e., AE energy, AE hits, AE count, and AE frequency etc. Kusunose et al. first applied the triaxial compression test to evidence the effect of two types of grain size rocks (fine and coarse granodiorites) on the character of AEs (Kusunose et al. 1991). Moreover, Lokajicek and Vik have obtained that the characteristic value of AE energy is directly proportional to the mean grain diameter (Lokajicek and Vik 1996). Přikryl et al. (2003) from the analysis of the experimental results concluded that stronger grains break at higher stresses and release more energy than the weak ones, besides, the microscopic fabric (i.e., grain size, shape, and preferred orientation of crystal), AE count and energy can better reflect the structural characteristics of rocks.

In summary, the effects of minerals composition and texture characteristics have been widely studied in previous research on the strength and AE signals characteristics of all three lithologies types (sedimentary, metamorphic, igneous). However, strength comparisons of three lithologies types are relatively rare. Besides, there is infrequent studying of the influence of rock minerals composition and texture characteristics on the AE signals (i.e., cumulative AE hit rate, cumulative AE count rate, cumulative AE energy). However, the rock strength and AE signals characteristics released from fissures and fractures expending and producing have a strong relationship with minerals composition and texture characteristics. Hence, in this paper, a correlation between rock mechanical properties (i.e., σ_c , σ_t , and

E) and AE signals and their mineral composition and grain size have been analyzed based on the testing of 13 different rock types with comparative methods. Moreover, the static parameters (i.e., P wave velocity, density, Schmidt hammer rebound value) of rocks were correlated using a simple regression analysis related to the mechanical parameters (i.e., σ_c , σ_p , and E). From the analysis of the results, the rocks minerals composition and texture characteristics can be used as predictive factors for rock strength. The AE signal characteristics can enhance the understanding of rock microstructure.

2 Experimental Methodology

2.1 Rock Specimen Preparation

In this paper, the origin places of 13 different types of test rocks in China were plotted, as shown in Fig. 1a, and two different kinds of rock specimens with a diameter of 50 mm were prepared. The rock specimens of 100 mm length were used for UCT, whereas 30 mm length specimens were used for BIT, as shown in Fig. 1b. In Fig. 1b, the number 1–13 denotes Yunnan yellow sandstone, ZiGong white sandstone, JinJiang brown sandstone, LongChang green sandstone, WuDing red sandstone, ZiGong grey sandstone, JuNan purple sandstone, LeiYang fine marble, HeZhou coarse marble, ZhuMaDian metamorphic granite, MiLuo granite, LeiZhou fine granite, and Altai mountains andesite, respectively. In addition, the nondestructive indexes of the rocks were also determined before the destructive tests, i.e., density, P wave, and Schmidt Hammer rebound value (RHV). The Schmidt Hammer is a widely used method to estimate rock strength in geo-engineering. The values of different index properties are shown in Table 1. In Table 1, the rocks Nos. 1–7 are sedimentary rocks, No. 8–9 are metamorphic rocks, and Nos. 10–13 are igneous rocks. Compared with the three types of rocks, the density, P wave, and Schmidt Hammer rebound value (RHV) of igneous rock, metamorphic rock and sedimentary rock decrease once.

2.2 Petrographic Descriptions

The 13 different rocks selected in this paper were grouped into three different categories, i.e., metamorphic, igneous and sedimentary rocks. Two thin sections were prepared for each of the rocks, one perpendicular to the core plane (VCP) and one parallel to the core plane (PCP) to get a better view of the mineral composition and grain size of the rocks used in this study, specific test steps can be referred to Geological and Mineral Industry standards of the People's Republic of China DZ/T 0275.4-2015 (Ministry of Land and Resources 2015). Specification identification of

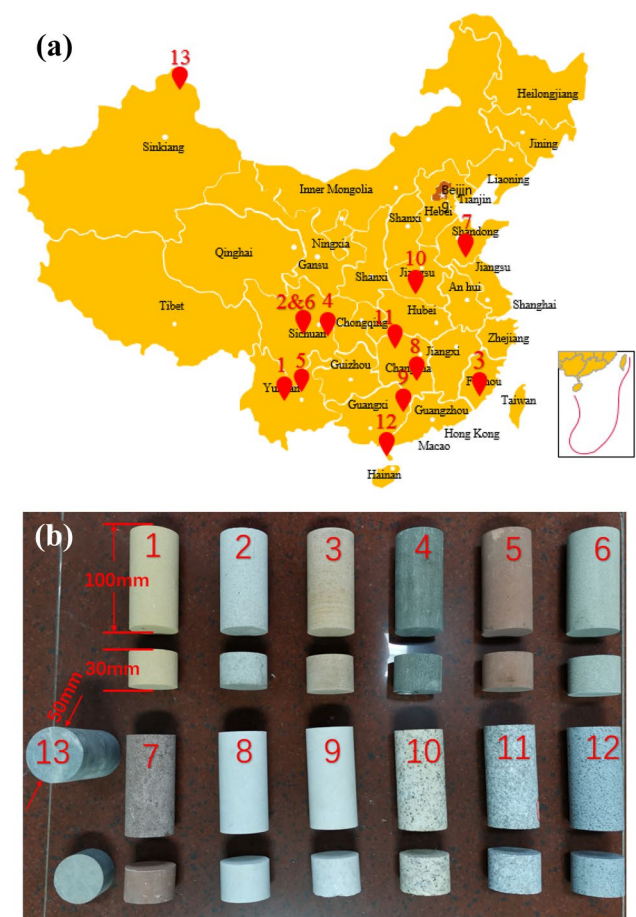


Fig. 1 Rock specimens used in this study

rock and mineral-Part 4: Thin section identification of rock (DZ/T 0275.4-2015). The micrographs of a thin section of six typical rocks are shown in Fig. 2. The six typical rocks and their petrographic properties (crystal shape, texture type, grain size) are shown in Table 2. The percentages of the 13 different rocks mineral components and mineral grain size statistics are shown in Tables 3 and 4, respectively.

The mineral component bar chart for each of the rocks was drawn and shown in Fig. 3. It can be observed that the top-three minerals in mass percentage are plagioclase, quartz, and K-feldspar, respectively. The total percentage of the three minerals is 89% for YunNan yellow sandstone, 78% for ZiGong white sandstone, 95% for JinJiang brown sandstone, 77% for LongChang green sandstone, 64% for WuDing red sandstone, 53% for ZiGong grey sandstone, 63% for JuNan purple sandstone, 92% for ZhuMaDian metamorphic granite, 81% for MiLuo granite, 72% for LeiZhou fine granite, 49% for Altai mountains andesite.

Table 1 Density (D), P wave velocity (V_p), and Schmidt Hammer rebound value (SHV) of the tested rocks

Rock no.	Rock name	Color	Categories lithology	D (g/cm ³)	V_p (m/s)	SHV
1	YunNan yellow sandstone	Yellow	Sedimentary	2.08	1679.53	31.5
2	ZiGong white sandstone	White	Sedimentary	2.32	2640.84	39.0
3	JinJiang brown sandstone	Brown	Sedimentary	2.19	1510.65	42.5
4	LongChang green sandstone	Green	Sedimentary	2.31	3297.71	47.5
5	WuDing red sandstone	Red	Sedimentary	2.4	3293.89	40.0
6	ZiGong grey sandstone	Grey	Sedimentary	2.58	3834.35	49.0
7	JuNan purple sandstone	Purple	Sedimentary	2.41	3293.89	47.5
8	LeiYang fine marble	White	Metamorphic	2.69	4201.49	33.0
9	HeZhou coarse marble	White	Metamorphic	2.82	3688.97	42.5
10	ZhuMaDian metamorphic granite	Yellow–black	Igneous	2.58	3433.45	48.0
11	MiLuo granite	White–black	Igneous	2.64	4337.18	46.5
12	LeiZhou fine granite	Grey–black	Igneous	2.79	5548.90	60.5
13	Altai mountains andesite	Grey–green	Igneous	2.83	6392.77	53.0

2.3 Experimental Apparatus and Testing Method

The uniaxial compression tests and Brazilian tension tests were performed using an MTS 322 T-shaped testing machine in the Advanced Testing Research Center, Central South University, A PC-II acoustic emission testing system was used to collect the AE signals during the whole loading process of each testing, as shown in Fig. 4. The loading rate in the two-testing series was set as 0.12 mm/min, as shown in Fig. 4b. The basic mechanical strength

parameters (i.e., σ_c , σ_t , and E) and the macro failure mode of rocks were obtained through the two-testing series. In this study, two AE sensors were used on each of the rock specimens, and the position of the sensors was geometrically symmetrical on the rock specimen. To receive better quality AE signals, the sensor was fixed by an iron ring attached to the rock surface with a magnetic cap (Du et al. 2020).

In order to reduce the impact of end friction on test results. Anti-friction measurement was carried out for each

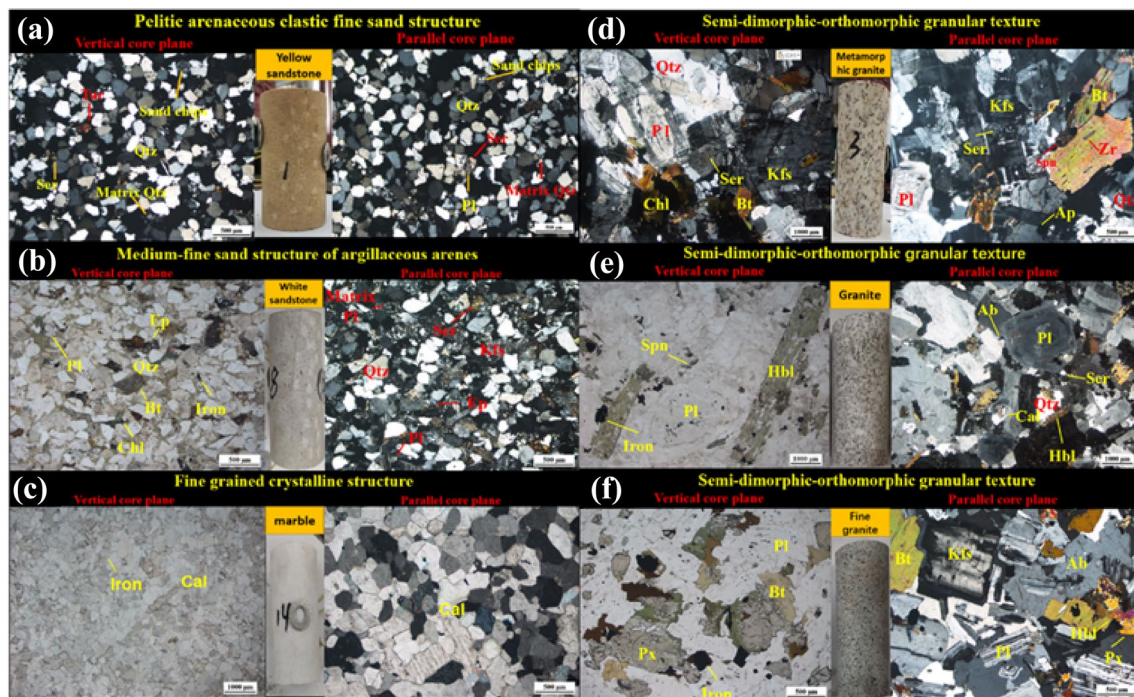


Fig. 2 Mineral thin section micrograph: **a** No. 1 Rock YunNan yellow sandstone, **b** No. 2 Rock ZiGong white sandstone, **c** No. 8 Rock LeiYang fine marble, **d** No. 10 Rock ZhuMaDian metamorphic granite, **e** No. 11 Rock MiLuo granite, **f** No. 12 Rock LeiZhou fine granites

group of samples. The detailed steps were as follows: (1) The Vaseline and polythene sheets with a circular section of 55 mm diameter were prepared; (2) Cleaning the two loading surfaces of specimens, and then evenly applying the first layer of Vaseline, and sticking the first layer of polythene sheet on the first layer of Vaseline. (3) Applying the second layer of Vaseline evenly on the first layer of polythene sheet, and then sticking the second layer of polythene sheet on the second layer of Vaseline.

3 Experimental Results

3.1 Mechanical Properties

3.1.1 Basic Mechanical Parameters

The uniaxial compressive strength (σ_c), tensile strength (σ_t) and elastic modulus (E) of the tested rocks are shown in Table 5. Uniaxial compressive strength σ_c , Tensile strength

(σ_t) and elastic modulus E (the ratio of stress and strain at 50% of peak stress), were calculated as Eqs. 1–3, respectively.

$$\sigma_c = \frac{P}{A} \quad (1)$$

$$\sigma_t = -\frac{2P}{\pi dh} \quad (2)$$

$$E = \frac{\sigma_{a2} - \sigma_{a1}}{\varepsilon_2 - \varepsilon_1} \quad (3)$$

where P is the maximum force value, A is the cross-sectional area of the specimen, d is the diameter of the specimen, h is the height of the specimen, σ_{a1} and σ_{a2} are the axial force corresponding to any two points of the line segment, ε_1 and ε_2 is strain corresponding to σ_{a1} and σ_{a2} .

Table 2 Petrographic descriptive statistics of six typical rocks

Rock no.	Rocks	Petrographic description
1	YunNan yellow sandstone	Irregular granular, angular–subangular, scattered plagioclase; Irregular granular, fine sandy, angular–subangular, smooth surface, visible quartz, recrystallized enhanced edge quartz; Irregular, subangular, fine-grained, mainly silicon cuttings; Dust-like, light-yellow–brown, iron irregular granular
2	ZiGong white sandstone	Irregular, subangular, fine-grained arenaceous; Irregular granular, medium-fine sandy, angular, smooth surface, wavy matte quartz; Irregularly grainy, medium-fine sandy, angular, surface fuzzy plagioclase; Irregular granular, medium-fine sandy, angular, latticed double crystal and striated potash feldspar; scaly, pale green chlorite; scaly sericite; argillaceous material is dust shape, light yellow–brown; irregular granular argillaceous and iron
8	LeiYang fine marble	Irregular granular, fine grain alloying structure, cleavage development, high-grade white interference color calcite; Irregular granular, microcrystalline, smooth surface, wavy extinction, scattered distribution of quartz; Irregularly granular iron
10	ZhuMaDian metamorphic granite	Semi-autochthonous plate, medium-fine grain, cleavage, and polycrystalline double, growth ring structure plagioclase; semi-automorphic–heteromorphic granular structure, medium-fine grain, developed lattice double crystal and striated potassium feldspar; Irregular granular, medium-fine grained, smooth surface, wavelike extinction, vermicular quartz; flaky, brown, with a group of highly fully cleavage biotite; scaly, pale green, unusually blue-interfered chlorite; flake, flake Muscovite (Ms), and sericite (Ser)
11	MiLuo granite	Semi-autochthonous plate, fine to medium grain, with a clean edge structure of plagioclase; semi-autochthonous-other-shaped structure, fine-medium grain, discernible texture and striated potassium feldspar; Irregular granular, smooth surface, wavy extinction quartz; Irregular granular, along with the grain edge metasomatism plagioclase and potassium feldspar, surface clean sodium feldspar; semi-autochthonous-other columnar, greenish-brown green, mainly medium grain, long columnar, rhombic crystal cross-section hornblende; semi-dimorphic granular with diamond crystal section sphene; Irregular granular, metasomatic plagioclase, potash feldspar, and hornblende, high-grade white interference calcite
12	LeiZhou fine granite	Semi-autochthonous plate, fine grain, cleavage, and polycrystalline double, a clean edge structure of plagioclase; Irregular granular, surface clean sodium feldspar; semi-autochthonous granular structure, visible striated potassium feldspar; Irregular granular, visible pyroxene cleavage pyroxene; Irregular granular, greenish-brown green, visible amphibole cleavage amphibole; flake, tan biotite; Irregular granular, smooth surface, wavy extinction quartz; semi-autochthonous-grainy, partially visible in square or hexagonal sections, and may be pyrite (Py) or magnetite (Mt)

Table 3 Mineral composition of the rocks thin section tested

Rock no.	Pl (%)	Qtz (%)	Kfs (%)	Bt (%)	Ms (%)	Zo (%)	Ser (%)	Chl (%)	Cal (%)	Ep (%)	Ir (%)	Sc (%)	Ab (%)	Hbl (%)	Spn (%)	Px (%)
1	2	87			0.5		0.5	-			5	5				
2	1	73	3		-		3	4	-		1	15				
3	11	72	12	0.5			2	0.5			2					
4	30	35	12	1.5	1.5	0.5	2	4	0.5		1	12				
5	12	42	10				2	2	12		8	12				
6	10	43		1	1		20	3	10			12				
7	20	33	10	-			1	-	4	-	6	25				
8		-			2			98			-					
9		-			2			98			-					
10	32	22	38	4	0.5	0.5	0.5	1	0.5		1				-	
11	38	18	25					1	2		3		5	5	3	
12	55	15	2	6				-			3		8	3		8
13	49						1	18	8		-		12			12

Table 4 Grain size of the rocks tested (unit: mm)

Rock no.	Pl	Qtz	Kfs	Bt	Ms	Zo	Ser	Chl	Cal	Ep	Ir	Sc	Ab	Hbl	Spn	Px
1	0.02-0.25	0.03-0.4			0.01-0.25		0.01-0.25	0-0.05			0.002-0.2	0.05-0.3				
2	0.05-0.4	0.05-0.7	0.05-0.4		0.01-0.2		0-0.05	0-0.05	0.01-0.05		0.002-0.2	0.05-0.6				
3	0.02-0.25	0.01-0.32	0.02-0.25	0.01-0.15			0-0.05	0-0.05			0.002-0.2					
4	0.05-0.6	0.02-0.5	0.05-0.45	0.05-0.4	0.05-0.4	0.01-0.2	0-0.1	0-0.1	0.02-0.3		0.002-0.15	0.05-0.4				
5	0.02-0.3	0.01-0.5	0.02-0.4				0-0.05	0-0.05	0.01-0.2		0.002-0.2	0.05-0.4				
6	0.02-0.25	0.05-0.4		0.01-0.3	0.01-0.3		0-0.1	0-0.05	0.01-0.3		0.05-0.3					
7	0.02-0.7	0.05-1.2	0.05-0.7	0.01-0.1			0-0.05	0-0.05	0.05-0.45	0.01-0.2	0.002-0.4	0.1-1.8				
8		0-0.05						0.05-1.2			0.002-0.01					
9		0.01-0.06			0-0.1			0.02-3.4			0.002-0.2					
10	0.05-3.2	0.01-3.6	0.1-4.6	0.05-0.3	0-0.1	0.01-0.1	0-0.1	0-0.1	0.01-0.1	0.01-0.1	0.002-0.3				0.05-0.5	
11	0.1-3.6	0.05-1.2	0.1-3.2					0-0.1	0.01-0.3		0.002-0.7		0.1-1.2	0.02-3.0	0.05-1.4	
12	0.1-2.2	0.01-1.2	0.2-0.8	0.04-2.2				0.01-0.1		0.01-0.2	0.002-0.4		0.1-1.2	0.02-0.5		0.05-1.5
13	0.01-02.4						0-0.05	0-0.1		0.01-0.8	0.002-0.1					0.1-1.5

Pl Plagioclase, Qtz Quartz, Kfs K-feldspar, Bt Biotite, Ms Muscovite, Zo Zoisite, Ser Sericite, Chl Chlorite, Cal Calcite, Ep Epidote, Ir Iron, Sc Sand chips, Ab Albite, Hbl Hornblende, Spn Sphene, Px Pyroxene

Fig. 3 Mineral percentage of rocks

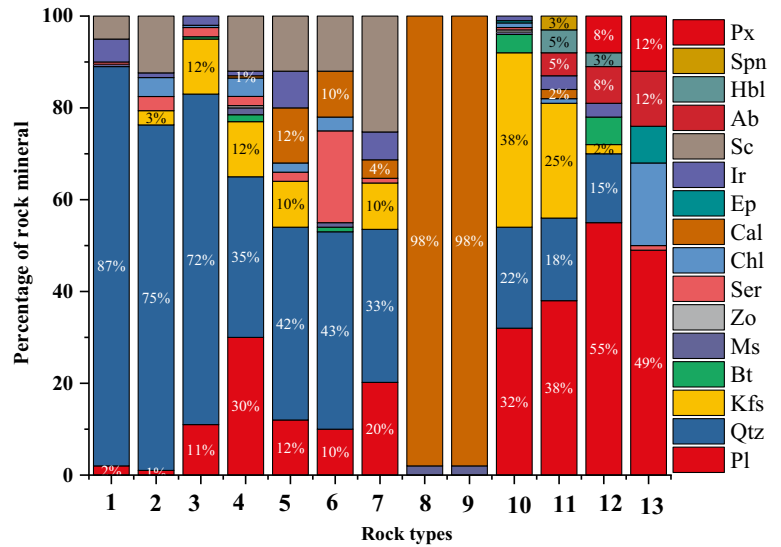
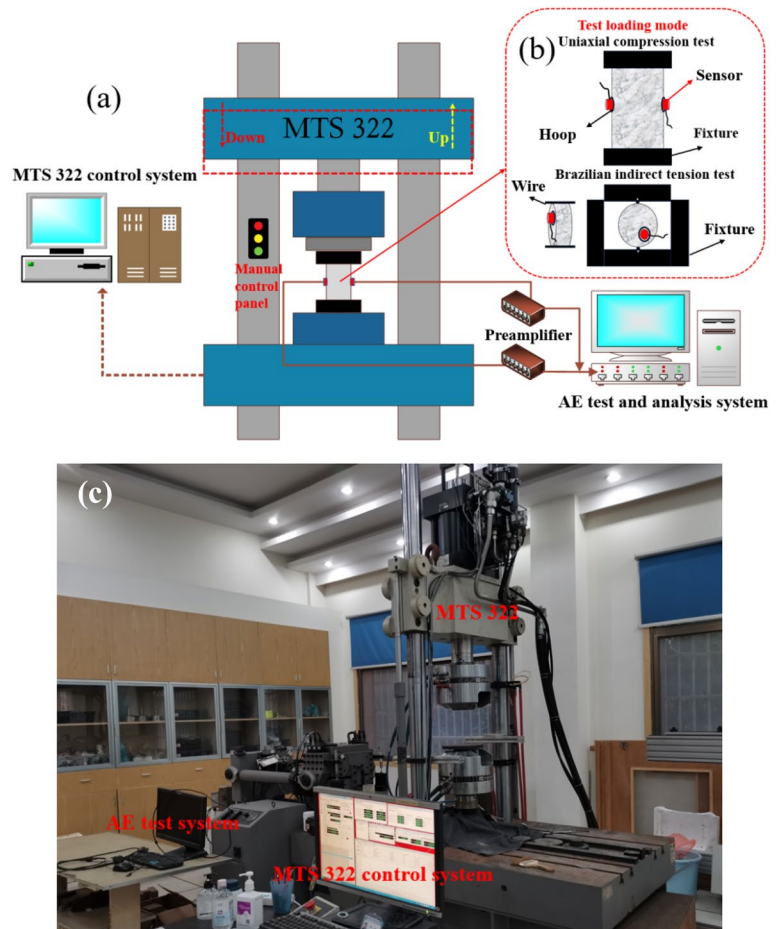


Fig. 4 MTS 322 testing machine and AE digital system



3.1.2 Relationships Between Mechanical Parameters and Nondestructive Index

The fitting curves of the nondestructive index [Density, *P* wave velocity *V_p*, Schmidt Hammer rebound value (SHV)]

with σ_c , σ_t and *E* are shown in Fig. 5. It is proved that *P* wave velocity, density, and elastic modulus *E* are important indexes to reflect the rock strength properties (Přikryl et al. 2003). From Fig. 5, it can be inferred that the density, *P* wave velocity *V_p*, and Schmidt Hammer rebound hardness value

Table 5 Uniaxial compressive strength (σ_c), tensile strength (σ_t) and elastic modulus (E) of the tested rocks

Rock no.	Uniaxial compressive strength σ_c (MPa)	Tensile strength σ_t (MPa)	Elastic modulus E (GPa)
1	45.0	1.4	83.93
2	39.0	1.6	76.45
3	67.3	3.4	79.99
4	69.2	2.6	15.31
5	75.0	2.8	11.10
6	76.8	3.0	12.36
7	92.8	4.3	17.09
8	49.0	2.9	18.35
9	99.2	2.7	20.16
10	70.3	3.5	11.10
11	114.7	7.8	22.65
12	155.4	8.5	55.37
13	193.4	14.7	36.23

(SHV) are positively correlated with the basic mechanical strength parameters of rocks.

3.1.3 Stress–Strain and Force–Displacement Curves

The stress–strain curves in uniaxial compression tests and the displacement–force curves in Brazilian tension tests of six typical rocks are shown in Figs. 6, 7, respectively. The σ_c and σ_t of three igneous rocks, i.e., LeiZhou fine granite, MiLuo granite and ZhuMaDian metamorphic granite, are significantly higher than that of the metamorphic and sedimentary rocks. In addition, the curves of the igneous rocks indicate more brittleness in their failure, whereas the sedimentary rocks have a greater plastic deformation stage and indicate more ductility of their failure.

3.1.4 Energy Evolution Characteristics of Rocks

Energy evolution through the whole process of rock deformation and failure, and is one of the effective ways to reveal the rock fracture process and rock mechanical properties. As a commonly used rockburst bursting energy evaluation index under uniaxial compression, bursting energy index W_{cf} is a rockburst evaluation method considering pre-peak and post-peak energy evolution (Zhou et al. 2018; Wang et al. 2021; Wen et al. 2021). This index can not only reflect the intensity of rock failure, but also reveal the process of rock failure energy accumulation and dissipation. W_{cf} is the ratio of accumulated deformation energy A_S to dissipated deformation energy A_X ; A_S is the area bounded by the stress–strain curve and the axis before the peak point of the stress–strain curve; A_X is the area bounded by the stress–strain curve and

the axis after the peak point of the stress–strain curve, were calculated as Eqs. 4–6, respectively. The schematic diagram of energy parameter calculation is shown in Fig. 8.

$$W_{cf} = \frac{A_S}{A_X} \quad (4)$$

$$A_S = \int_0^{\varepsilon_p} f(\varepsilon) d\varepsilon \quad (5)$$

$$A_X = \int_{\varepsilon_p}^{\varepsilon_F} f(\varepsilon) d\varepsilon \quad (6)$$

where ε_p is the total strain in the comprehensive loading curve; ε_F is the strain before pre-peak strength in the comprehensive loading curve.

The accumulated deformation energy A_S , dissipated deformation energy A_X and bursting energy index W_{cf} calculation results and variation trend of six typical rocks are shown in Table 6 and Fig. 9, respectively. According to the calculated results, the accumulated deformation energy A_S of igneous rocks is more than 200 kJ/m³, which is much larger than that of sedimentary and metamorphic rocks, and the dissipated deformation energy A_X of the three types of rocks are little different. Therefore, it can be considered that part of the energy of igneous rocks is used for internal dissipation of rocks, and most of the energy is converted into kinetic energy of rocks, while for sedimentary and metamorphic rocks, the amount of energy converted into kinetic energy of rocks is much smaller. This well explains the experimental phenomenon that igneous rock is stronger than sedimentary and metamorphic rocks in the moment of failure. In addition, the bursting energy index W_{cf} of LeiZhou fine granite exceeds 5 (heavy bursting liability with $W_{cf} > 5$, weak bursting liability with $1.5 \leq W_{cf} < 5$, no bursting liability with $W_{cf} < 1.5$), and it is the only one with heavy bursting liability among the 6 rock species, while the other rocks can be evaluated as a weak or medium bursting liability.

3.2 AE Characteristics

In this part, six typical rocks, i.e., YunNan yellow sandstone for No. 1, ZiGong white sandstone for No. 2, LeiYang fine marble for No. 8, ZhuMaDian metamorphic granite for No. 10, MiLuo granite for No. 11, LeiZhou fine granite for No. 12, were selected to analyze the AF–RA density, AE peak frequency, AE hit rate, b value, AE count rate and cumulative AE hit, AE energy, and AE cumulative energy of AE signals in the two series tests. In the next section, the six typical rocks are replaced with rock numbers. The AE signals of the two AE sensors were similar, so the AE data of one AE sensor was selected in the analysis in this paper.

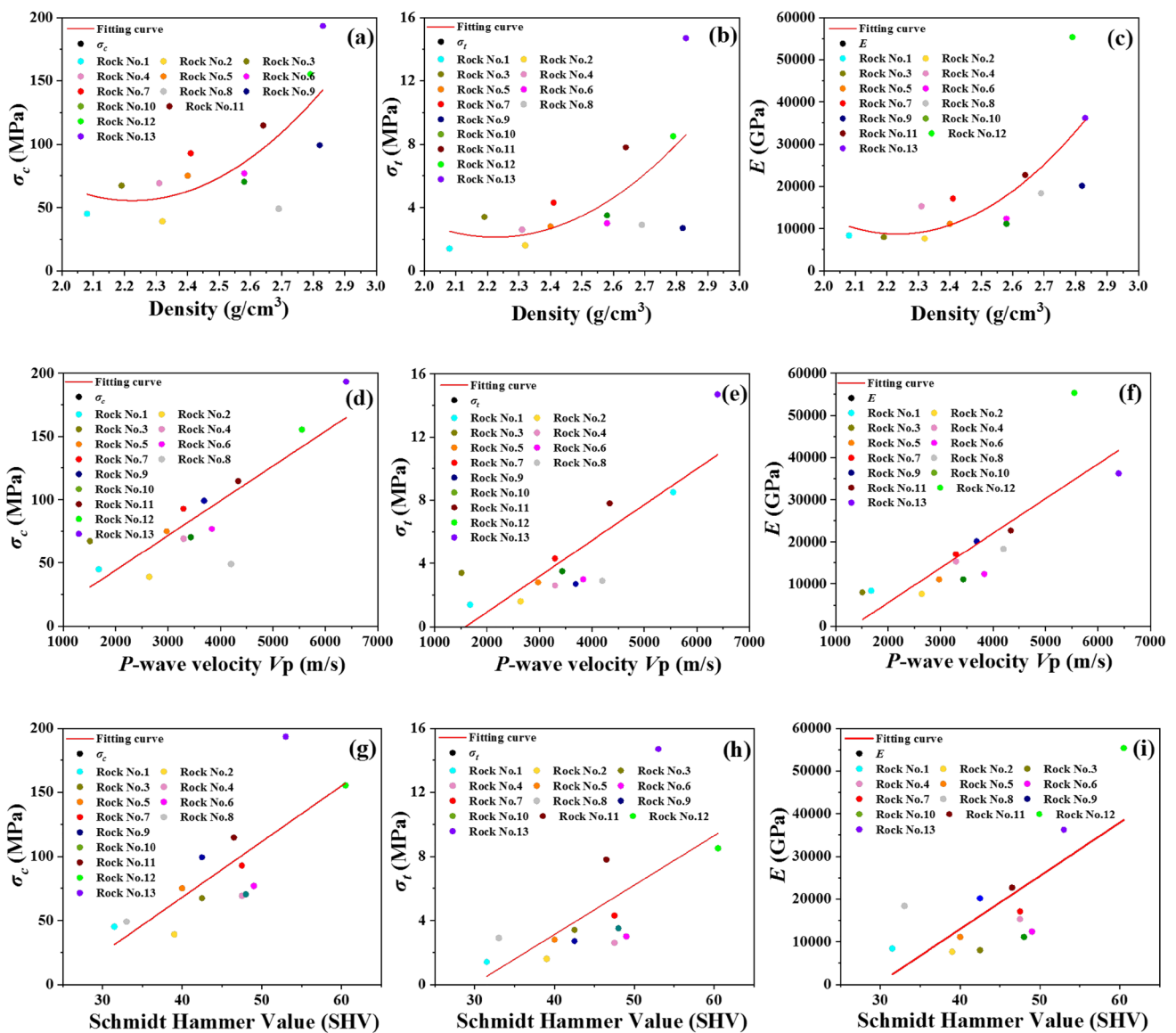


Fig. 5 Relationship between mechanical parameters and nondestructive index: **a-c** density; **d-f** *P* wave velocity V_p ; **g-i** Schmidt Hammer (SH) rebound hardness value (SHV)

The parameter AF is the average frequency of the AE waveform and RA is the ratio of the rise time to amplitude. The AE hit rate and AE count rate refer to cumulative AE hit and AE count of the specimens in one second during the process of rock failure. The cumulative count hit and energy are the sum of the whole data of these signals during the process of loading.

In addition, the *b* value reflects the relationship between the frequency and magnitude of earthquakes proposed firstly by Gutenberg and Richter in 1944 (Gutenberg 1944), as per Eq. (7). In the case of the AE study, Eq. (8) can be modified as Eq. (8) using AE parameters (Rao 2005). Moreover, the *b* value represents the percentage of low amplitude AE hits in comparison to the high

amplitude AE hits, which means that a large *b* value indicates a larger proportion of low amplitude AE hits. In this study, the *b* value is a dynamic *b* value, which is to divide the disturbance time equally by taking the beginning and end of each disturbance stage as nodes. The main conclusions based on the AE data analysis are as follows:

$$\lg N = a - bM \tag{7}$$

$$\lg N(A/20) = a - b(A/20) \tag{8}$$

where *M* is the magnitude of earthquakes, *N* is the cumulative number of earthquakes with a magnitude of *M*, *A* is the amplitude of the AE hits, and *N* is the cumulative number

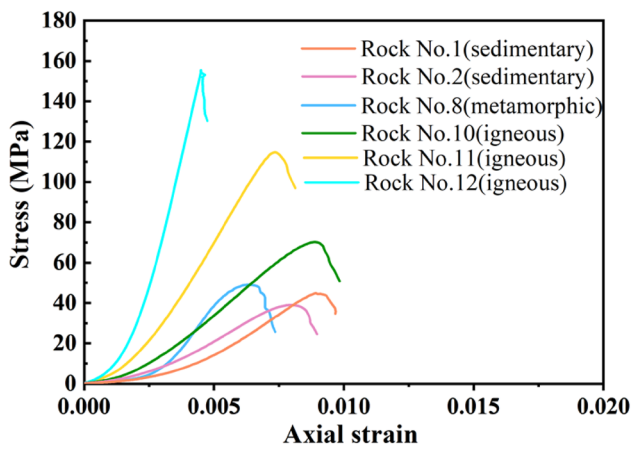


Fig. 6 UCT stress–strain curves

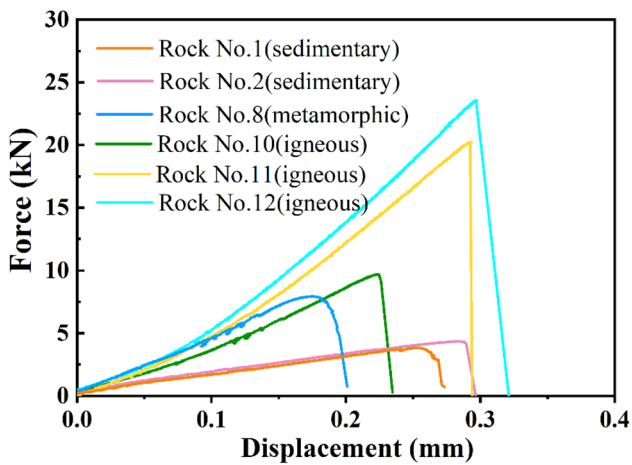


Fig. 7 BIT force–displacement curves

of AE hits with an amplitude of A , a and b are empirical constants.

3.2.1 AF–RA Density

In this part, the AF–RA nuclear density and scatter maps have been drawn to analyze the AF–RA distribution laws of the uniaxial compressive test and Brazilian tension test. The normalized AF–RA nuclear density maps are also given to study AF–RA distribution laws under the same outline standard. Moreover, the fractured images of rocks in UCT and BIT are shown, which clearly reflect the damage pattern of the rocks. In the AF–RA nuclear density map, the data density gradient rises from red to blue to purple. Besides, the area with higher nuclear density and scatter values have been circled with white and black dashed lines. Figures 10, 11, 12 show the results of YunNan yellow sandstone for rock

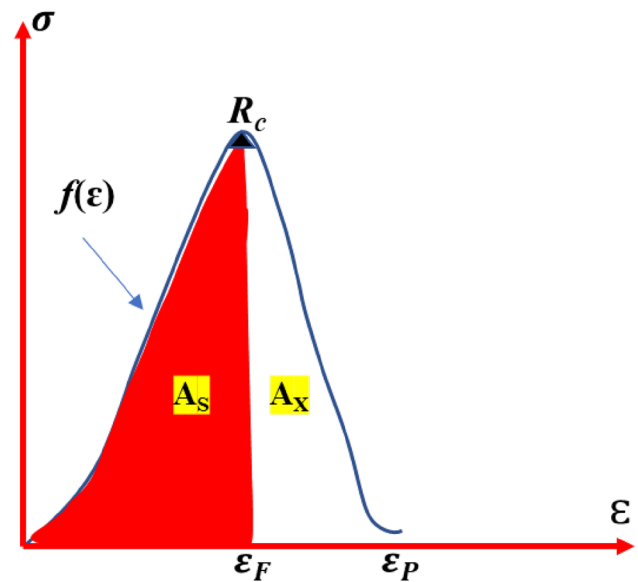


Fig. 8 Schematic diagram of energy parameter calculation

No. 1 and ZiGong white sandstone for rock No. 2, LeiYang fine marble for No. 8 and ZhuMaDian metamorphic granite for No. 10, and LeiZhou fine granite for No. 11, and MiLuo granite for No. 12, respectively.

In the AF–RA density distribution characteristics of the six kinds of rocks under the uniaxial compression test, the AF–RA distribution characteristics of LeiZhou fine granite are different from the other five kinds of rocks. From the Figs. 8, 9, 10, it can be concluded that the other five rocks' AF–RA and normalized AF–RA data are mainly distributed below 100 kHz and 0.2, respectively, and the five rocks (rocks Nos. 1, 2, 8, 10, 12) have a wide distribution range for RA but narrow for AF. These five rocks' RA is mostly ranging from 0 to $20 \times 10^5 \mu\text{s/V}$ and the MiLuo granites' RA is greater than $30 \times 10^5 \mu\text{s/V}$, while AF is mostly in the 0–100 kHz range. Besides, these rocks data are mostly near the RA axis with a long side in density maps and AF data are mainly below 200 kHz in scatter maps.

In addition, according to rocks fractured images, it can be said that these five rocks failed with many large-angle cracks. For instance, the ZhuMaDian metamorphic granite failed with a single large-angle shear crack with an angle of nearly 70° , which clearly shows that rock failed in shear. But for LeiZhou fine granite, the data of AF–RA and normalized AF–RA are mostly distributed ranging from 100 to 400 kHz and from 0.2 to 0.4, respectively, and are mostly near the AF axis with a long side and the values mostly exceed 200 kHz. From the LeiZhou fine granite failure image, the vertical cracks are in majority, which indicates that the rock failed in tension. Furthermore, under the Brazilian indirect tension test, all of the typical rocks have a widely distributed range for AF but narrow for RA, and the results are the same as

Table 6 The accumulated deformation energy A_S , dissipated deformation energy A_X and bursting energy index W_{cf} of six typical rocks

Rock no.	Rocks	Categories lithology	Accumulated deformation energy A_S (kJ/m ³)	Dissipated deformation energy A_X (kJ/m ³)	Bursting energy index W_{cf}
1	YunNan yellow sandstone	Sedimentary	133	32	4.1
2	ZiGong white sandstone133	Sedimentary	130	47	2.8
8	LeiYang fine marble	Metamorphic	145	42	3.5
10	ZhuMaDian metamorphic granite	Igneous	273	60	4.6
11	MiLuo granite	Igneous	354	84	4.2
12	LeiZhou fine granite	Igneous	236	35	6.7

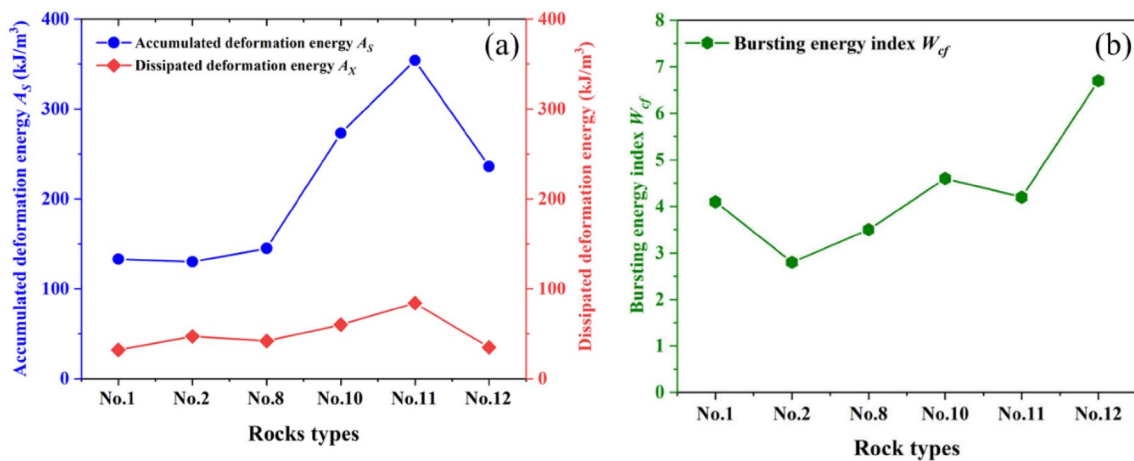


Fig. 9 Variation of energy parameters of six types of rocks

LeiZhou fine granite but opposite to the other five rocks. The AF data mostly range from 100 to 400 kHz and RA data mostly range from 0 to 10×10^5 μ s/V. It is well known that the rocks were dominated by tension damage in Brazilian tension tests.

To sum up, according to the above analysis, these five typical rocks (rock No. 1,2,8,10,12) are shear failures with widely RA with a long side but narrow AF distribution, the AF is mostly distributed in 0–100 kHz. Different from other rocks, the LeiZhou fine granite has a widely AF but narrow RA distribution, failed by tension, and the AF data are mostly distributed at 100–400 kHz. Hence, applying acoustic emission technology can effectively predict the main failure mode of rock, which has certain theoretical guidance for engineering practice.

3.2.2 AE Peak Frequency

Figure 13 shows the AE peak frequency pie charts in UCT and BIT for the six typical rock types. According to Fig. 13, the proportion of AE peak frequency range from 0 to 100 kHz is 89.51% for rock No. 1, 90.07% for rock No.

2, 78.6% for rock No. 8, 86.08% for rock No. 10, 20.94% for rock No. 11, 85.1% for rock No. 12 in uniaxial compressive test. It is clear that, except for LeiZhou fine granites, the AE peak frequency of rocks is mostly concentrated on 0–100 kHz. However, for the Brazilian tension test, the proportion of AE peak frequency range from 200 to 400 kHz is 59.14% for rock No. 1, 50.13% for rock No. 2, 91.42% for rock No. 8, 77.67% for rock No. 10, 56.13% for rock No. 11, 80.79% for rock No. 12. It can be concluded that the peak frequency in BIT is basically distributed between 200 and 400 kHz and the result is the same as the LeiZhou fine granites in UCT. So, combined with the conclusions reached in Sect. 3.2.1, the LeiZhou fine granites is failed in tension in UCT but the other five rocks (Nos. 1, 2, 8, 10, 12) in shear, which can be resulted if the AE peak frequency is mostly distributed below in 100 kHz, the rocks mainly failed in shear, but if the AE peak frequency is mostly distributed 200–400 kHz, the rocks are dominated by tension damage. Therefore, it is also reliable to distinguish the major failure modes of rocks according to the distribution of AE peak frequency.

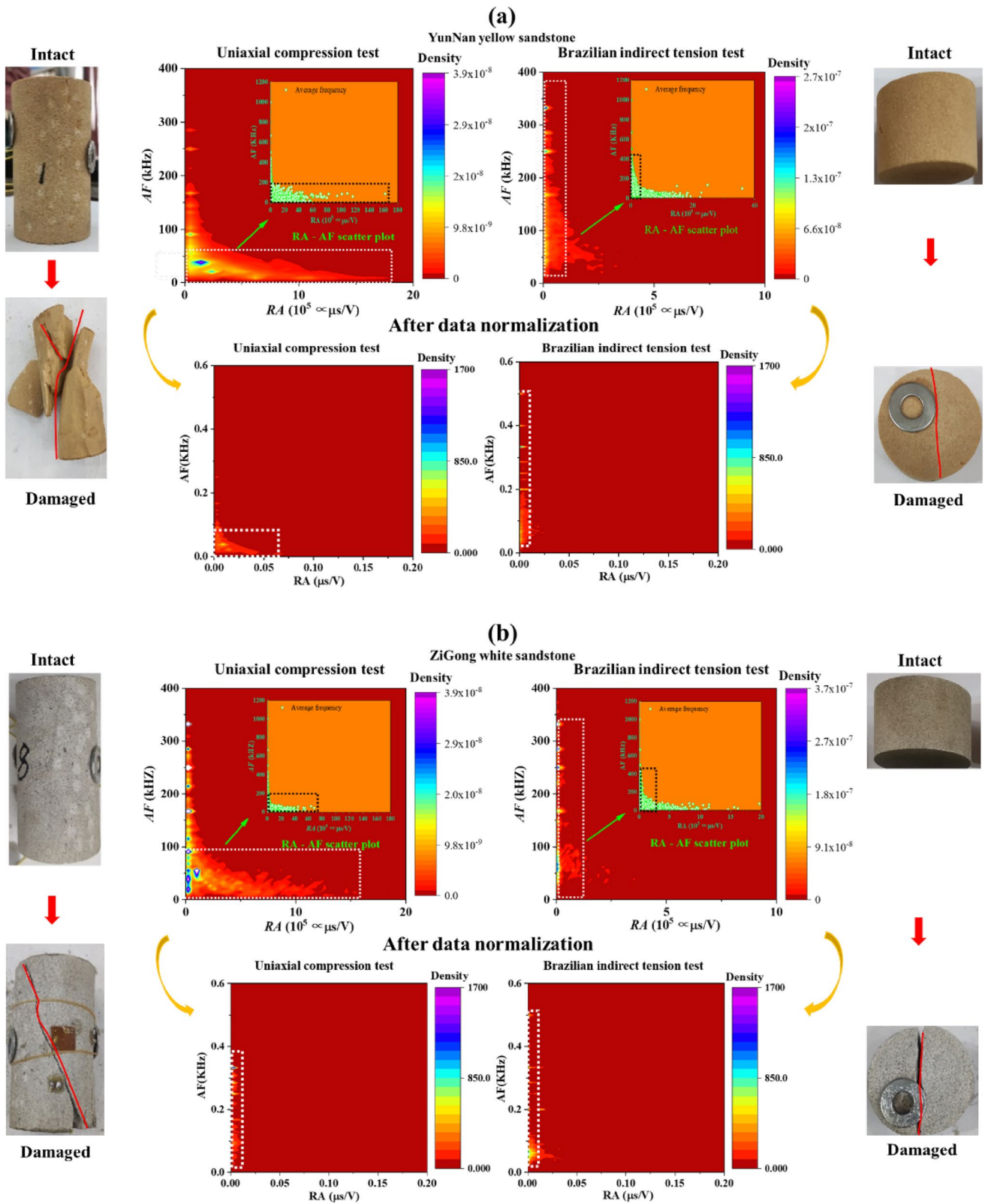
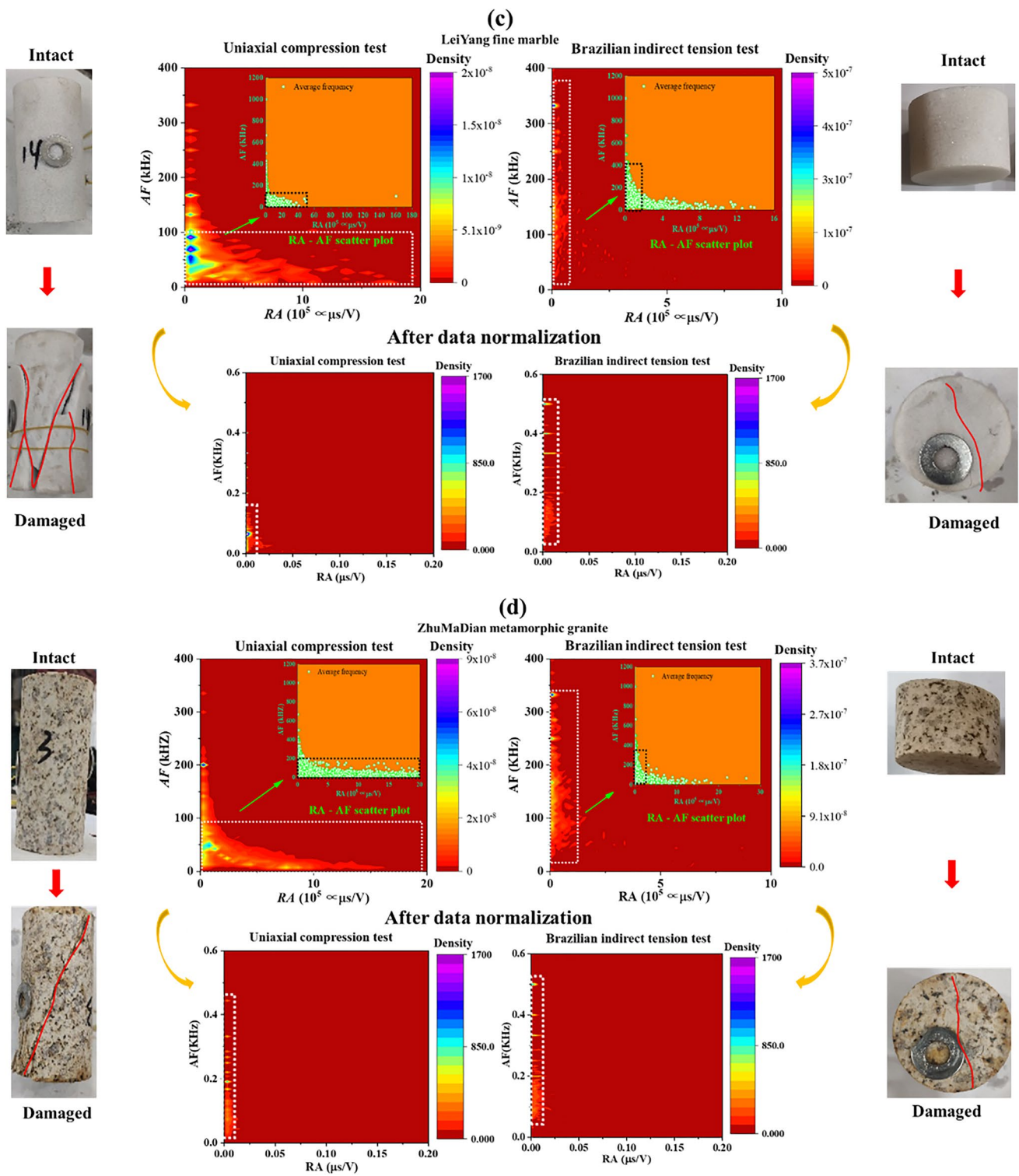


Fig. 10 *AF*–*RA* and normalization density, scatter plots, and pre-post failure graphs of UCT and BIT: **a** rock No. 1 (sedimentary); **b** rock No. 2 (sedimentary)



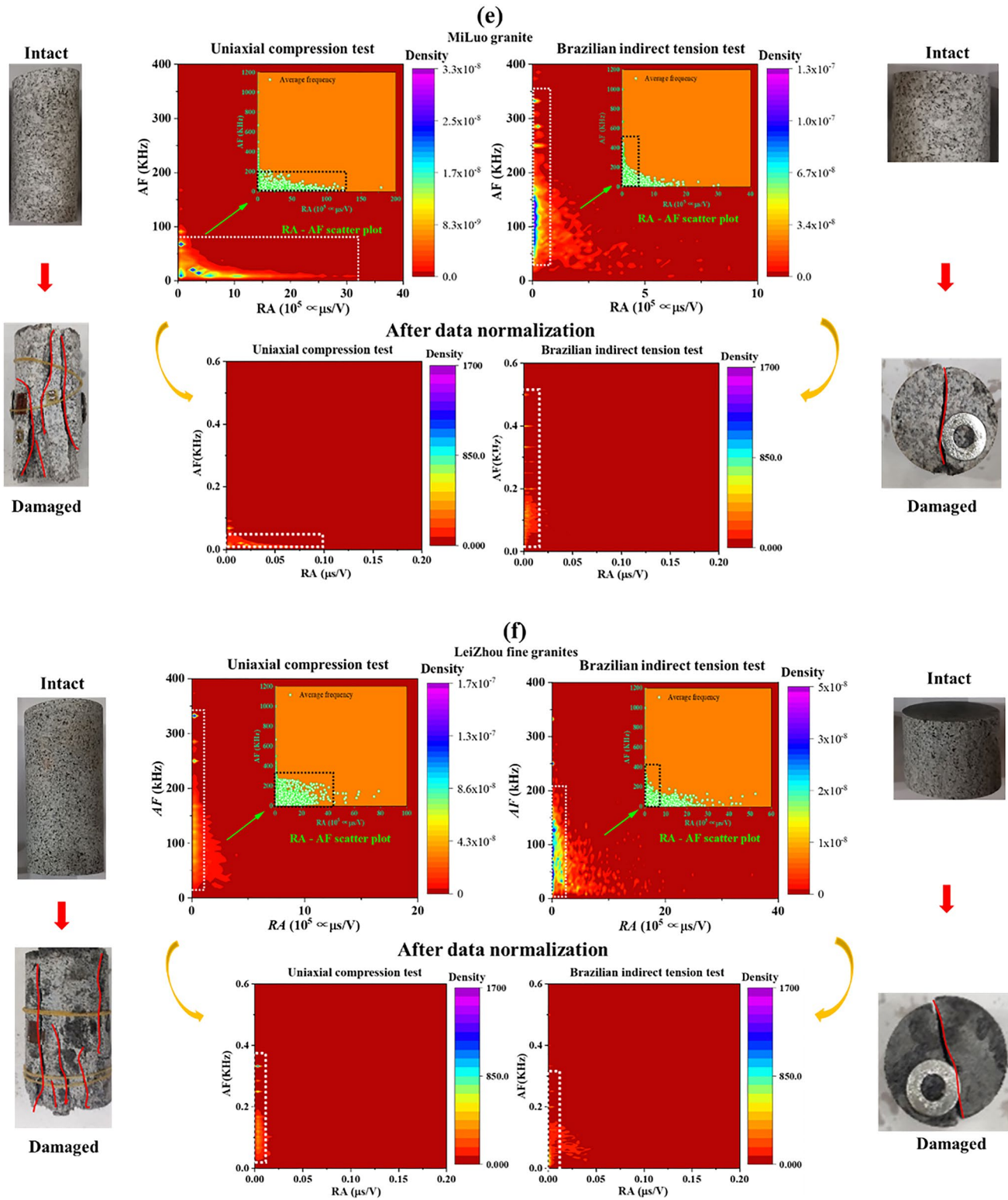


Fig. 12 AF-RA and normalization density, scatter plots, and pre-post failure graphs of UCT and BIT: **e** rock No. 11 (igneous); **f** rock No. 12 (igneous)

Fig. 13 AE peak frequency of UCT and BIT: **a** rock No. 1 (sedimentary); **b** rock No. 2 (sedimentary); **c** rock No. 8 (metamorphic); **d** rock No. 10 (igneous); **e** rock No. 11 (igneous); **f** rock No. 12 (igneous)

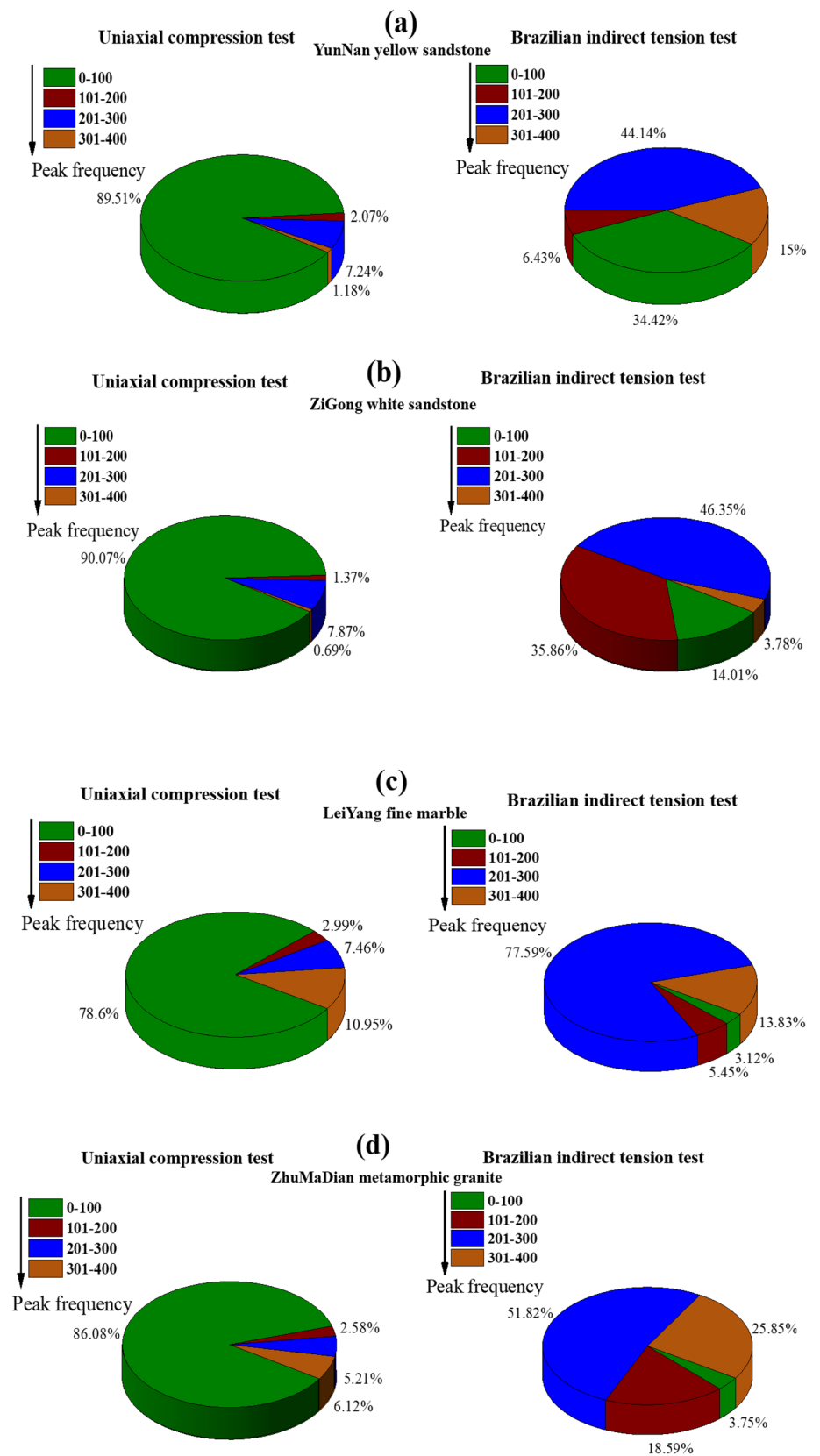
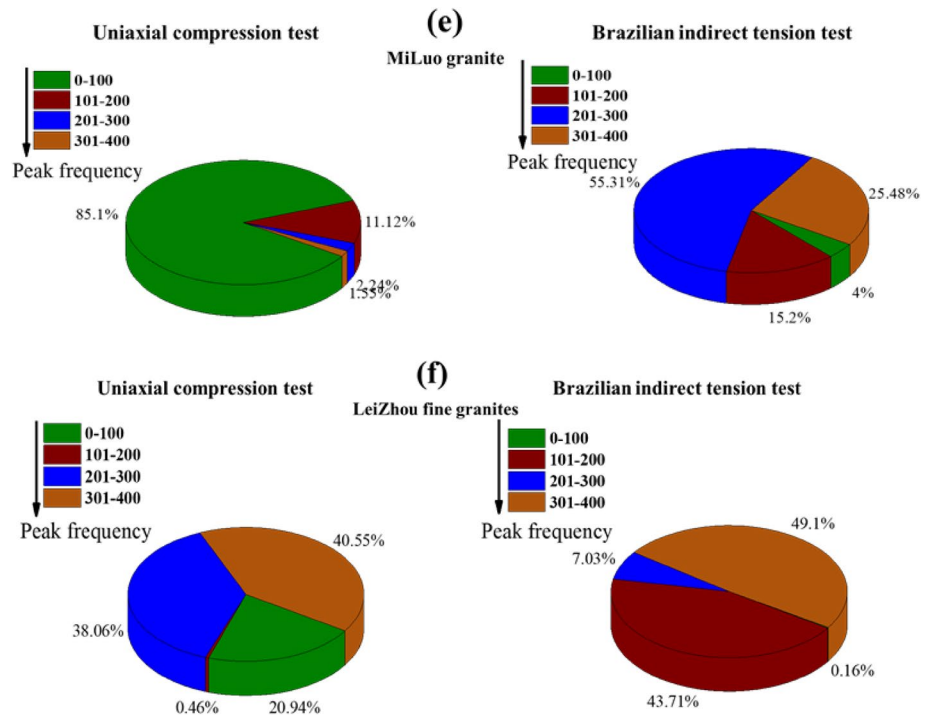


Fig. 13 (continued)



Moreover, the speed, number and size at which rocks produce fissures may also affect AE peak frequency. It can be observed from the experiments and fracture images that the fissures and cracks were in huge numbers and large sizes, which was accompanied by a high AE peak frequency in BIT. However, in UCT, the fissures and cracks appear slowly, few in numbers and smaller in size, which was accompanied by a low AE peak frequency.

3.2.3 *b* Value, AE Hit Rate, AE Count Rate and Cumulative AE Hit

It has been identified that AE count rate, AE hit rate and cumulative AE hit rate can reflect the intensity of the rock failure, including fracture size and number in loading. More, the *b* value can be used as a parameter index to predict rock failure. Thus, the six typical rocks trend of the *b* value, AE count rate, AE hit rate and cumulative AE hit rate over time and axial forces in UCT and BIT are shown in Fig. 14 and the AE signals are listed in Table 7.

Analysis from the lithology of the rocks, the maximum value of AE count rate of igneous rocks (rocks Nos. 10, 11, 12) in UCT is 166653, 206,296, 257,803, respectively, whose magnitude is about 10 times higher than that of both of the sedimentary rocks (rock No. 1 for 13,648 and rock No. 2 for 57,883) and metamorphic rocks (rock No. 8 for 31,502). Besides, it can also be observed that the maximum cumulative AE count rate of igneous rocks is about 10 times that of sedimentary rocks and metamorphic rocks, which is

almost the same conclusion as that of the AE count rate in UCT. However, six typical rocks in BIT of AE count rate peak value are 45,447 for No. 1, 22,524 for No. 2, 17,879 for No. 8, 49,870 for No. 10, 19,894 for No. 11, 106,357 for No. 12, and the AE hit rate peak value is 998 for No. 1, 768 for No. 2, 895 for No. 8, 654 for No. 10, 812 for No. 11, 673 for No. 12. So, it can be concluded that the peak values of the AE count rate and the AE hit rate of the three lithologies were about at the same magnitude level. At the same time, it is different compared to UCT about cumulative AE count rate and cumulative AE hit rate in three lithologies in BIT. There were no significant differences in the peak cumulative AE count rate of three lithologies in BIT. However, the peak cumulative AE hit rate of sedimentary rocks was greater than the igneous and metamorphic rocks.

From the AE signals change trend shown in Fig. 14, the first peak point of the AE count rate and AE hit rate appeared earlier and more frequently than the rocks in UCT in BIT. This phenomenon is more obvious in sedimentary rocks (sandstone), the results indicate that the crack grows rapidly and the macro fissure also forms rapidly in the BIT, which corresponds to the high peak value frequency phenomenon in the above conclusion. In UCT, there is a difference compared to the BIT, which is mostly AE count rate and AE hit rate peak value points of rocks appeared instantaneously before and after the rock failure. In addition, the AE signals were less in the early stages of UCT, which can be attributed to the fact that the rock cracks appear less due to the compaction stage. Therefore, the crack development is slow in the early stage of UCT, whereas the crack growth

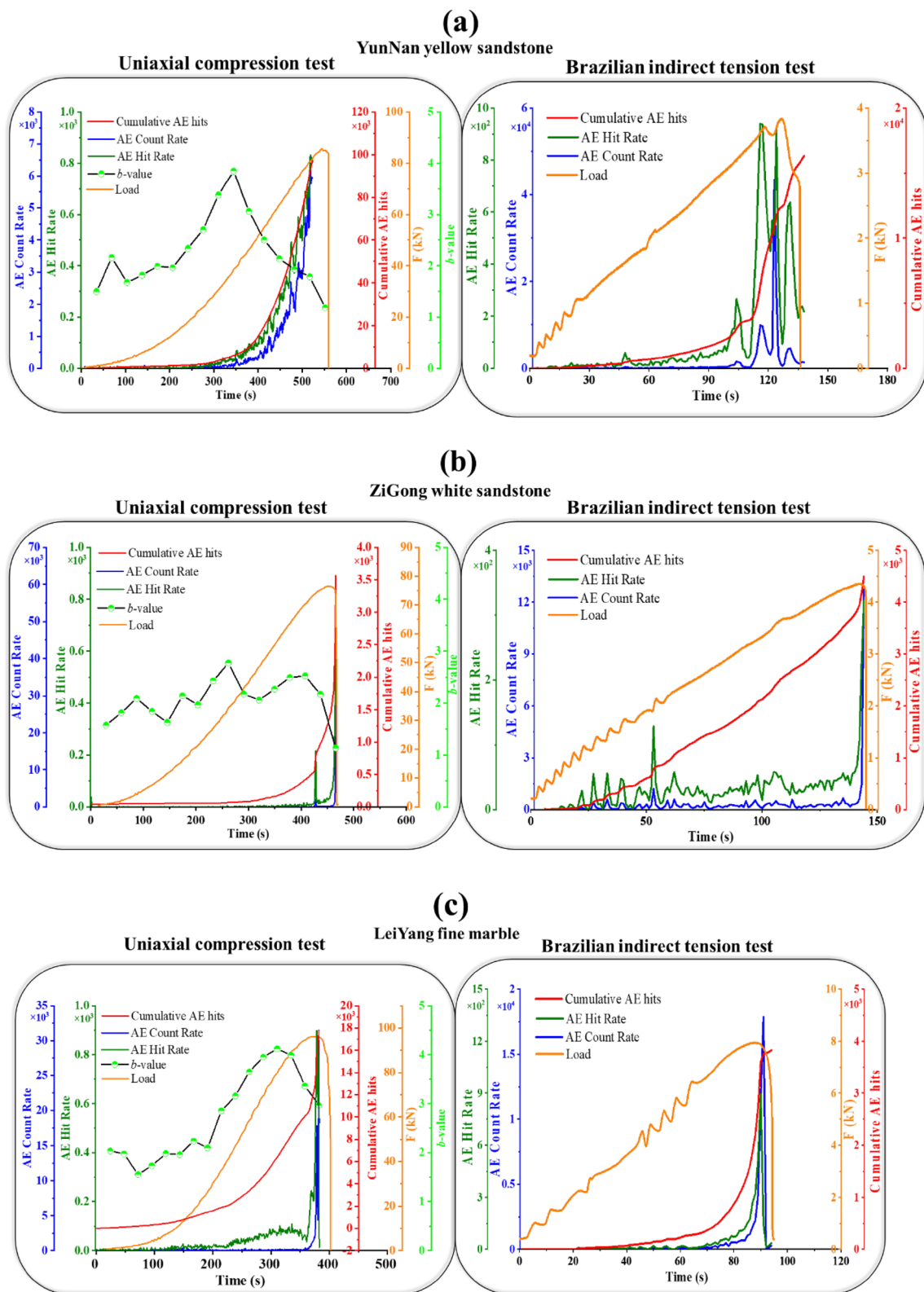


Fig. 14 AE count rate, AE hit rate, and cumulative AE hit rate of UCT and BIT: **a** rock No. 1 (sedimentary); **b** rock No. 2 (sedimentary); **c** rock No. 8 (metamorphic); **d** rock No. 10 (igneous); **e** rock No. 11 (igneous); **f** rock No. 12 (igneous)

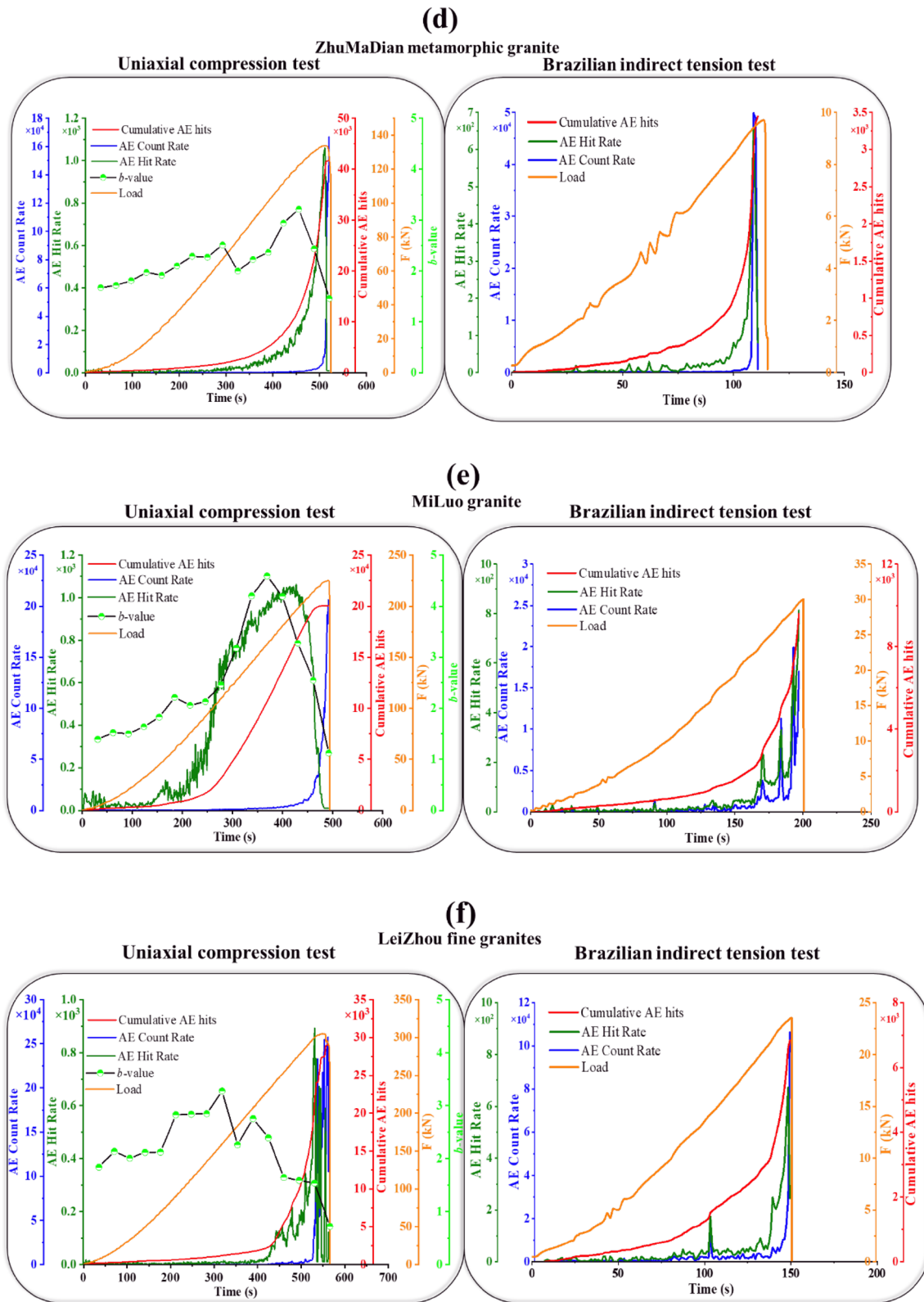


Fig. 14 (continued)

Table 7 The tendency of strength and AE signals

Rock no.	Categories	Strength (σ_c and σ_t) tendency			Mineral	AE tendency		
		Plagioclase	Quartz	k-feldspar		Cumulative AE hit rate	Cumulative AE count rate	Cumulative AE energy rate
1	Sedimentary	With plagioclase content increase, strength increase then decrease	With quartz content increase, strength (dropping slowly)	With k-feldspar content increase, strength then decrease	Plagioclase	With plagioclase increase, AE cumulative hit rate increase	With plagioclase increase, AE cumulative count rate increase then decrease	With plagioclase increase, AE cumulative hit rate increase
2								
3								
4								
5								
6								
7								
10	Igneous	With plagioclase content increase, strength increase	With quartz content increase, strength decrease (dropping rapidly)	With k-feldspar content increase, strength decrease (dropping slowly)	K-feldspar	With k-feldspar increase, cumulative AE hit, count, energy all increase then decrease		
11								
12								

is more intense before the rock failure. The crack propagates rapidly in BIT, and the AE signal is obvious throughout the whole test.

In addition, in terms of the overall trend of *b* values, the three types of rocks have similar trends, generally showing a trend of increasing first and then decreasing or a pattern of high in the middle and low on both sides. It is obvious that there is an obvious phenomenon of a sudden drop in *b* values before rock failure, which is consistent with the conclusion of previous studies.

In summary, the difference in lithology may be the main reason for the different AE signals, especially in UCT. The microstructure of rocks in different lithologies must be different, and the formation and expansion of the cracks in rocks under external stresses are often influenced by their mineralogy and texture characteristics. Moreover, the results have proved that the Acoustic emission (AE) technology can be used to analyze and evaluate rock fracture and crack propagation effectively and efficiently (Wang et al. 2016; Moradian et al. 2016). So, the AE signals may have a close correlation with rocks mineralogy and texture characteristics.

3.2.4 AE Energy and Cumulative Energy

The AE energy and the cumulative AE energy of six typical rocks are plotted, as shown in Fig. 15 and the AE data are presented in Table 7. In UCT, the cumulative energy of six typical rocks is 803771 mm*ms for rock No. 1, 14,162 mm*ms for rock No. 2, 39,202 mm*ms for rock

No. 8, 530,313 mm*ms for rock No. 10, 1,699,353 mm*ms for rock No. 11, 2,189,545 mm*ms for rock No. 12. The energy analysis results show that the cumulative AE energy of igneous rocks is greater than that of the other two lithologies, and the LeiZhou fine granite has the maximum cumulative energy value as well as the highest strength among the test rocks. The cumulative energy is increasing with its strength under the same rock lithology, especially in igneous. Similarly, it can be observed that the AE energy does not fluctuate greatly in the early stage of the uniaxial compression test, but is released suddenly before the rock failure. This phenomenon is extremely obvious in igneous rocks. The experimental phenomenon also indicated that the igneous rocks have a higher rock-burst trend. At the same time, by comparing the intensity of rocks failure with higher AE energy and lower AE energy and the size and classification of fragments after rocks failure, the quantity and size of failure cracks in rocks were estimated qualitatively. It can be found that the number and size of the cracks in specimens with higher AE energy are more and larger than those with lower energy after the rock failure. Therefore, it can be concluded that the energy accumulation of rocks with greater strength is more obvious under the action of compression external stress, which leads to a greater liability of rockburst and a higher degree of damage to the rocks. Similar conclusions were also found in both the compression and tension tests in AE hit rate for AE energy and cumulative AE energy,

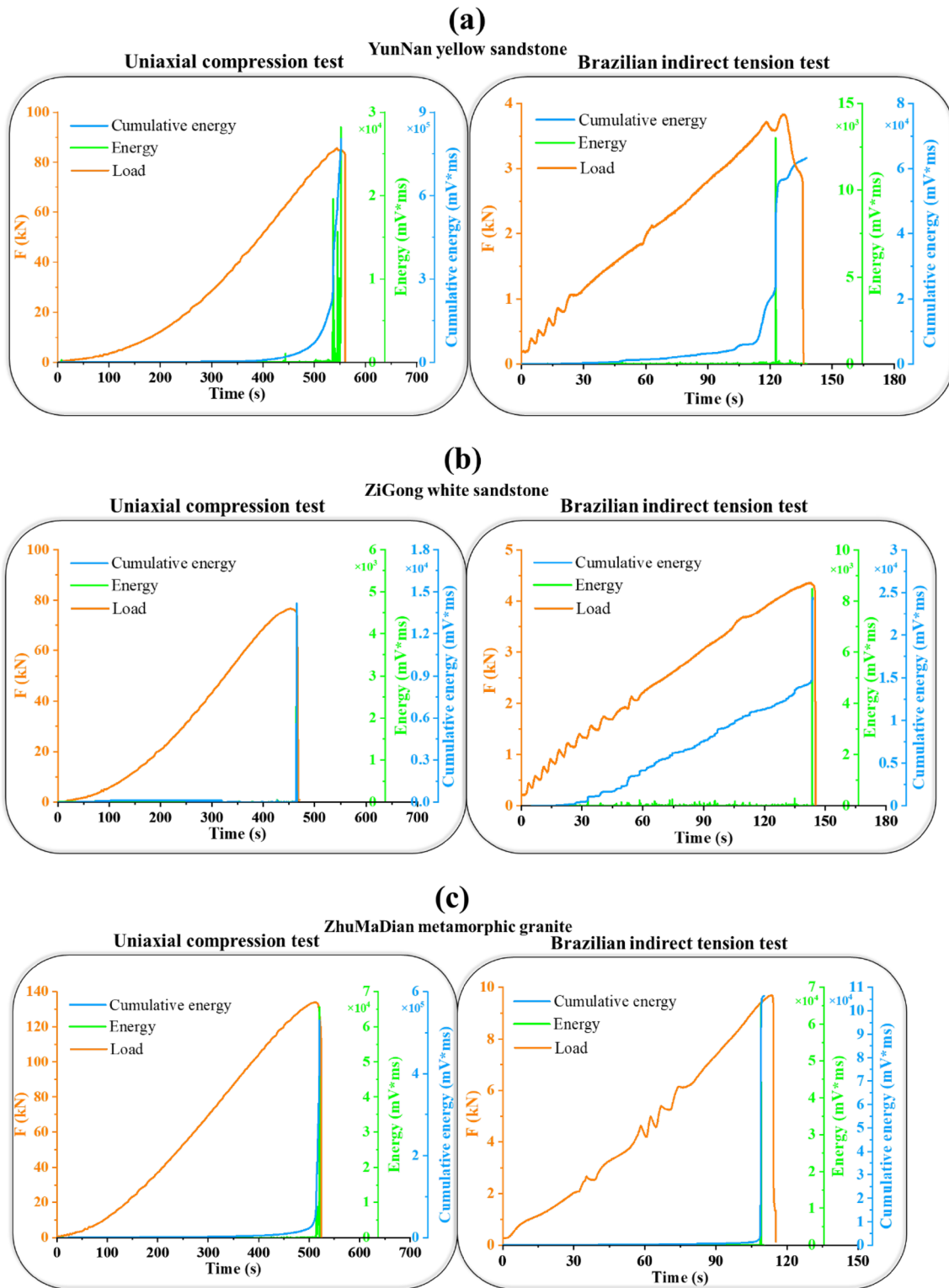


Fig. 15 Energy and Cumulative energy of UCT and BIT: **a** rock No. 1 (sedimentary); **b** rock No. 2 (sedimentary); **c** rock No. 8 (metamorphic); **d** rock No. 10 (igneous); **e** rock No. 11 (igneous); **f** rock No. 12 (igneous)

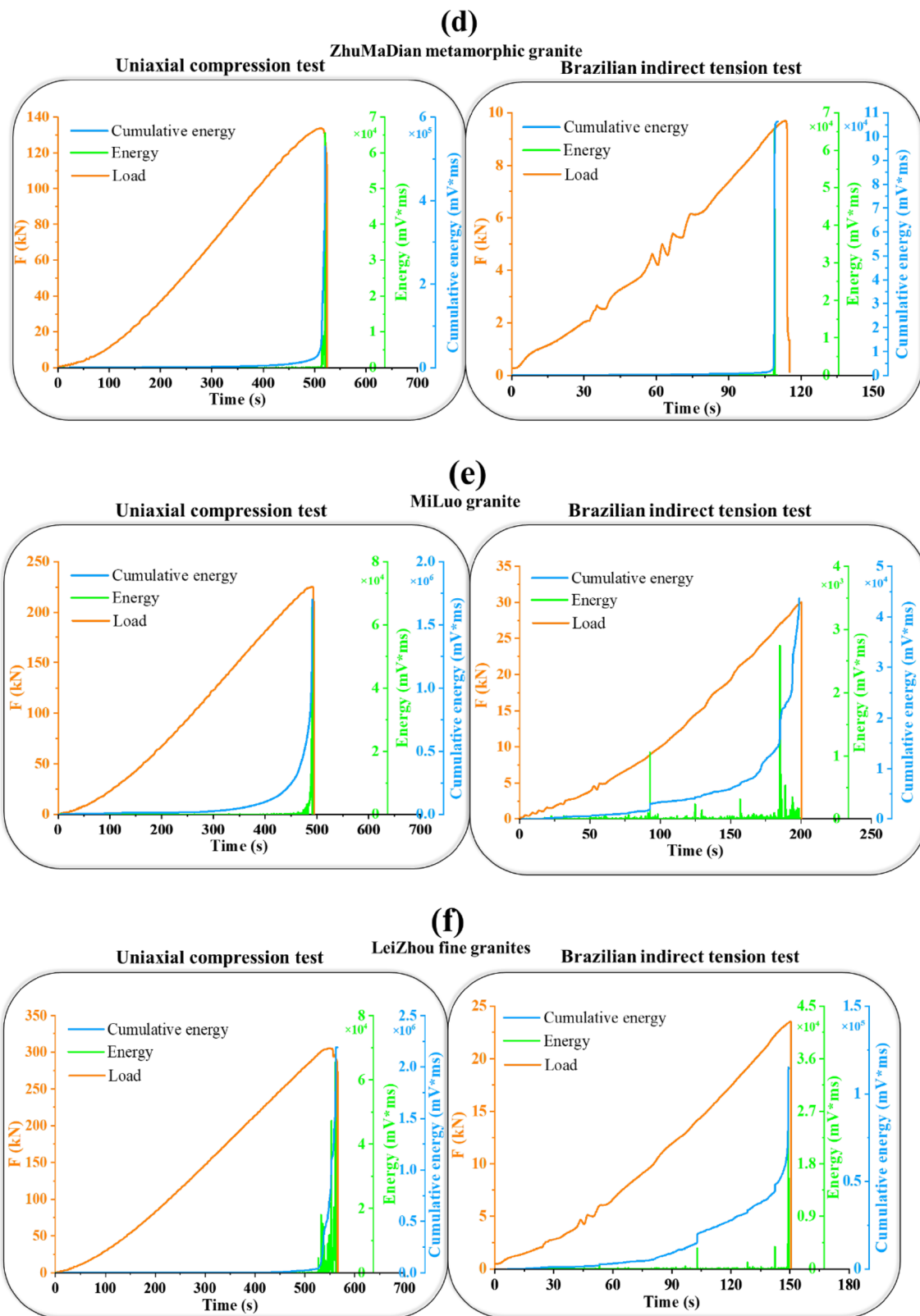


Fig. 15 (continued)

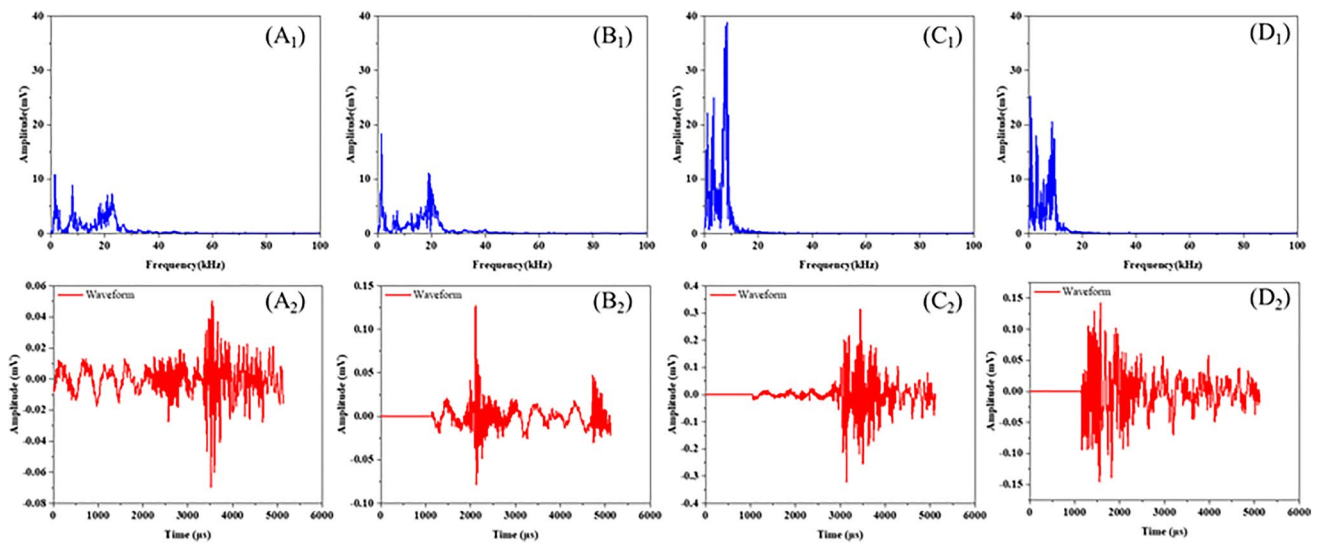


Fig. 16 YunNan yellow sandstone (sedimentary) original AE waveform and frequency domain characteristics

i.e., the AE energy peak value indicating the occurrence of rock failure.

3.2.5 AE Waveform Characteristics

Acoustic emission signal waveform analysis is a signal processing method to obtain material fault information by analyzing time–domain waveform. The time–domain waveform of the acoustic emission signal can be converted into the frequency domain by the Fourier transform of the waveform. In this study, YunNan yellow sandstone, LeiYang fine marble and MiLuo granite were selected as waveform analyses for sedimentary, metamorphic and igneous, respectively. Four

AE waveform signals are randomly selected for each rock sample in the same channel. The point selection principle is A and B with high AF value and low RA value, that AF is greater than or equal to 200 kHz, and RA is less than or equal to 5 s/V; C and D with low AF value and high RA value, that AF is less than or equal to 100 kHz, and RA is greater than or equal to 10 s/V.

The original AE waveform, frequency domain of YunNan yellow sandstone, LeiYang fine marble and MiLuo granite are shown in Figs. 16, 17, and 18, respectively. In the figure, the letter subscript 1 represents the relation between the frequency domain after the Fourier transform of a waveform, and the letter subscript 2 represents the

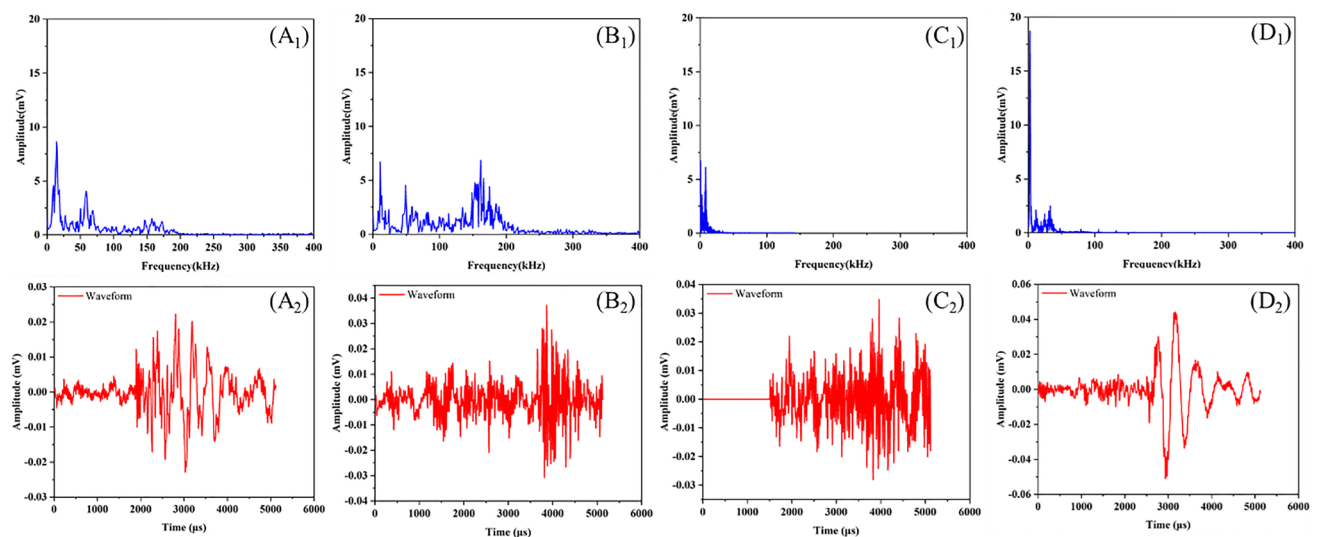


Fig. 17 LeiYang fine marble (metamorphic) original AE waveform and frequency domain characteristics

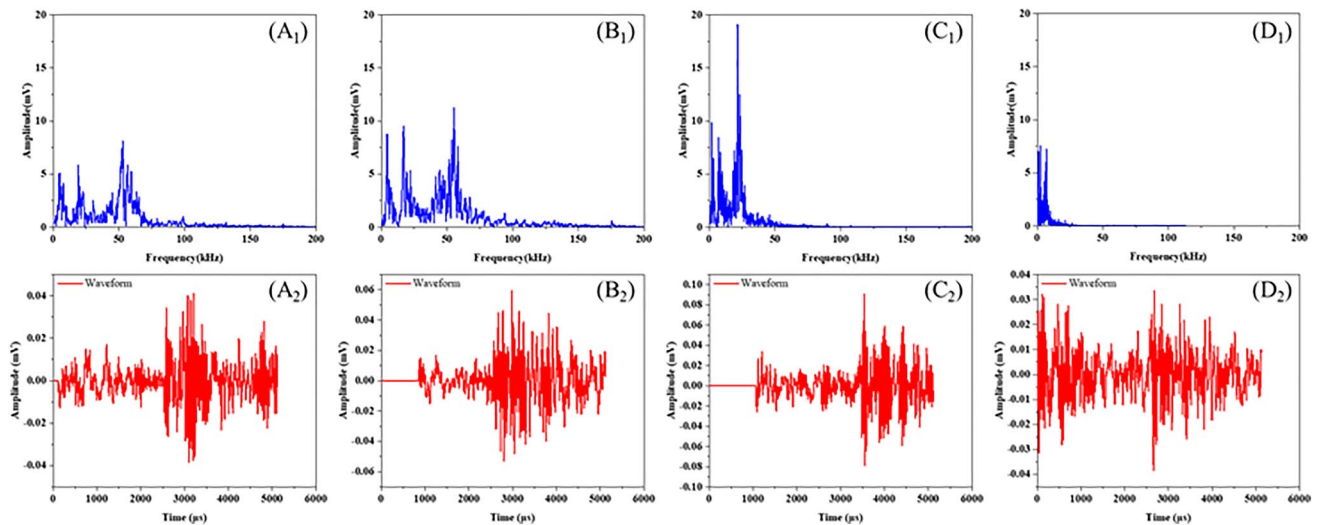


Fig. 18 MiLuo granite (igneous) original AE waveform and frequency domain characteristics

original AE waveform. By observing the frequency domain characteristics of the three types of rocks, it can be found that the frequency domain fluctuates in low amplitude and high frequency in Figures A_1 and B_1 , while C_1 and D_1 are mainly concentrated in low frequency or high amplitude. In addition, the values of frequency and amplitude in the AE frequency domain are also different for different lithologies. For example, for YunNan yellow sandstone, Fig. 16, the amplitude is less than 20 mV, frequency is less than 40 kHz of both A_1 and B_1 , which is different with A_1 and B_1 the amplitude is greater than 20 mV, frequency is less than 20 kHz of both C_1 and D_1 . But for LeiYang fine marble Fig. 17, the frequency domain mainly fluctuates in the range of frequency less than 200 kHz and amplitude less than 10 mV of both A_1 and B_1 , while the C_1 and D_1 frequency are mainly below 50 kHz.

Through the above analysis, it can be found that the high AF value and low RA value AE signals show the low amplitude and high-frequency characteristics, and the low AF value and high RA value AE signals show the high amplitude and low-frequency characteristics. According to the previous research results, tensile cracks are dominant in rocks with high AF values and low RA values, while shear cracks are dominant in rocks with low AF values and high RA values. Therefore, it can speculate that the frequency domain characteristics of low amplitude and high frequency are generated by tensile crack, and high amplitude and low frequency are generated by shear crack.

4 Discussion

The effects of plagioclase, quartz, and K-feldspar on rock strength and AE characteristics were discussed in detail. It is worth noting that white marble is mainly composed of Calcite, whereas other rock types contain lesser Calcite, so the Calcite influence on the rock mechanical properties is ignored in this part. At the same time, the proportion of plagioclase, quartz, and K-feldspar in Altai mountains andesite does not exceed 50%, thus, the Altai mountains andesite is also not discussed.

4.1 Mineral Composition and Grain Size Effects on Strength

To analyze the influence of the main minerals on σ_c and σ_t , the relationship between the percentage content of main rock minerals (i.e., plagioclase, quartz, and K-feldspar) with σ_c and σ_t was plotted and shown in Fig. 19, and the results are presented in Table 7. For better views, the sedimentary rocks and igneous rocks are connected by blue dotted lines and red dotted lines, respectively. From the Fig. 19a, it can be inferred that the plagioclase content in igneous rocks is higher than the sedimentary rocks, and the σ_c and σ_t increase first and then decreases with the increase of plagioclase content in sedimentary rocks, and the σ_c and σ_t of igneous rocks increase with the increase of the plagioclase content. The quartz content in igneous rocks is also higher than the sedimentary rocks, as shown in Fig. 19b. However, the σ_c and σ_t of rocks decrease as quartz content increases in igneous and sedimentary rocks. Moreover, as the quartz content increases, the reduction in igneous rocks strength is strong compared with the plagioclase and K-feldspar. From

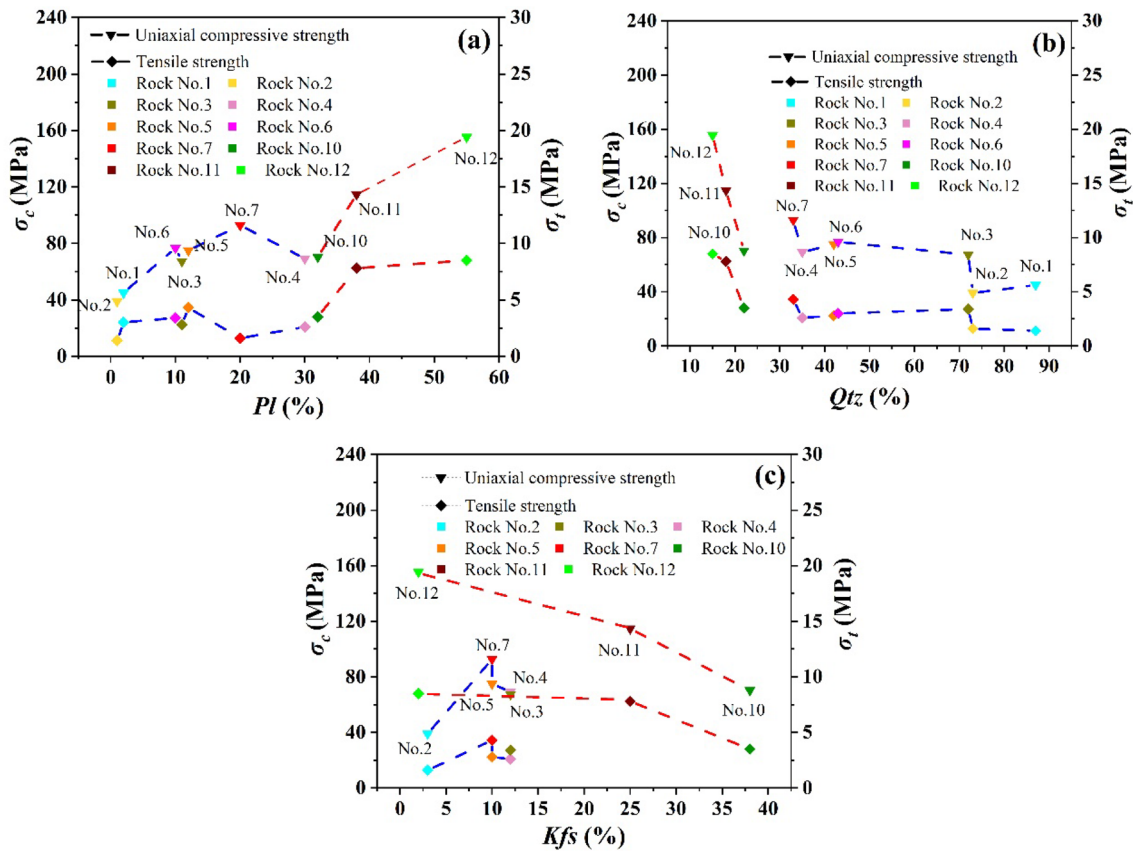


Fig. 19 Relationship between mineral percentage with σ_c and σ_t : a plagioclase; b quartz; c k-feldspar

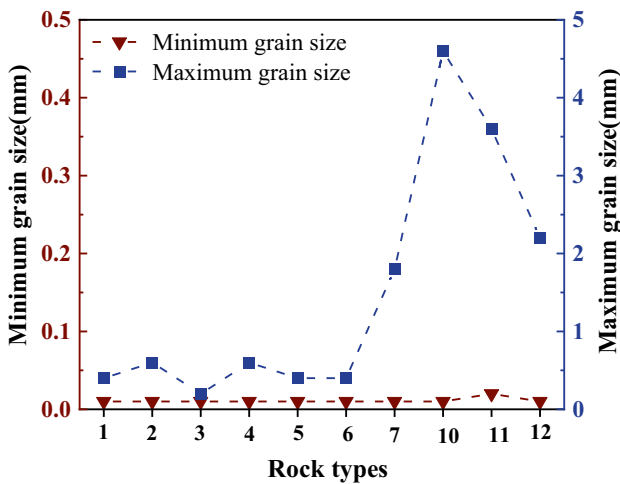


Fig. 20 Maximum and minimum mineral grain size of the tested rocks

Fig. 19c, the σ_c and σ_t of igneous rocks decrease with the increase of K-feldspar content, and the σ_c and σ_t of sedimentary rocks first increase and then decrease with the increase of K-feldspar content.

From the study, it can be concluded that different mineral components have clear impacts on the mechanical properties of rocks. The uniaxial compression strength σ_c and tensile strength σ_t of sedimentary and igneous rocks are positively correlated with the plagioclase content and negatively correlated with the quartz content. Furthermore, the quartz content has a strong weakening effect on the strength of igneous rocks. In conclusion, plagioclase has a strongly positive effect on the strength properties of rocks, whereas quartz has an opposite effect.

It is widely accepted that the maximum value of granularity distribution is called the typical value of granularity (Přikryl et al. 2003). Thus, the maximum and minimum particle diameters of the 10 rock types are drawn and shown in Fig. 20, and the relationship between the maximum particle diameter of main mineral components with σ_c or σ_t is shown in Fig. 21.

From the statistic, the minimum diameter of rocks is less than 0.1 mm, and the maximum diameter of sedimentary rocks is less than 1 mm except for JuNan purple sandstone (rock No. 7). However, for igneous rock Nos. 10, 11, and 12, the maximum diameter of grain sizes are 4.6 mm, 3.8 mm, and 2.2 mm, respectively, where grain size diameters are greater than the sedimentary rocks. The statistical analysis

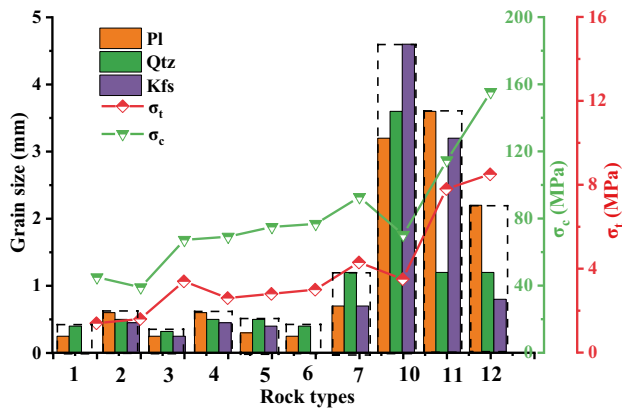


Fig. 21 Relationship between the grain size of main mineral components and σ_c or σ_t : (1) Rock No. 1, (2) Rock No. 2, (3) Rock No. 3, (4) Rock No. 4, (5) Rock No. 5, (6) Rock No. 6, (7) Rock No. 7, (8) Rock No. 10, (9) Rock No. 11, (10) Rock No. 12

results show that the maximum grain size diameter of sedimentary and metamorphic rocks used in this study is very small, and less than 0.08 mm, while the maximum grain size diameter of igneous rocks is comparatively much larger, as shown in Fig. 20. Presumably, if rocks mineral grains contain both coarse and fine grains, this diverse composition may increase the rock strength. It can also be observed in igneous rocks from Fig. 20 that the maximum diameter of plagioclase, quartz, and K-feldspar in rock No. 12 is the smallest among the rock numbers. 10, 11 and 12, whereas the rock No. 12 strength is the largest. Nevertheless, there is no clear regularity between the rock's strength and their mineral grain sizes in sedimentary rocks.

The analysis results can be obtained by correlating strength and mineral grain sizes. It can be said that the smaller the grain size is, the stronger the rock strength is. The rich particle size compositions may also increase the rock strength.

4.2 Mineral Composition and Grain Size Effects on AE Properties

According to the above analysis results, the correlation between AE signals and mineral composition is worth deeply studying. The statistics of AE count rate, cumulative AE count rate, AE hit rate and cumulative AE hit rate, energy and cumulative energy are used to study the relationship between mineral composition and AE signals characteristics, as presented in Table 8 and the results are listed in Table 7. The mineral content and cumulative AE count rate, cumulative AE hit rate and cumulative energy relation curves of UCT and BIT are illustrated in Figs. 22 and 23, respectively. It can be found that UCT and BIT are basically similar laws to AE accumulated energy

and K-feldspar content, except that there is a different law in the relationship between AE accumulated energy and K-feldspar content. Owing to BIT and UCT with similar laws, only UCT AE data can be analyzed below.

From the data analysis, it can be observed that the cumulative AE count rate and cumulative energy increase with the increase of plagioclase content, whereas with the increase of quartz content, the cumulative AE count rate and cumulative energy initially decrease and then increase. With the increase in K-feldspar content, the value of cumulative AE count rate and cumulative energy shows an increasing trend initially and then decreasing trend, which is different with the plagioclase and quartz. The relation between the three types of mineral content and cumulative AE hit rate increases first and then decreases. It is worth noting that the mineral content and AE characteristics laws are the same as between mineral composition and rock strength. These results proved that AE signals characteristics have a close relationship with rock strength.

To analyze the mineral grain size and AE signals correlation, the AE characteristics and maximum mineral grain size relations are plotted in Fig. 24. The results demonstrated that the three mineral's cumulative AE count rate and cumulative energy of rock with small grain size are significantly smaller than the large-size grains. These findings are similar to the conclusions obtained by Wang et al. (2016), that the fracture of larger grain rock under high stress releases more AE energy than the smaller grain under low stress. While the correlation between the cumulative AE hit rate and particle size is not significant.

As per Fig. 15, the plagioclase content is higher in igneous rocks compared to the other lithologies rocks, and the LeiZhou fine-grain granite for rock No. 12 contained the highest plagioclase content of more than 50%. From the analysis results of LeiZhou fine granite, the plagioclase content is the highest compared with the other two minerals, and the three main minerals grain size is smaller than the two igneous rocks (No. 11 and rock No. 12). Therefore, all these conditions may be the reasons for the high cumulative energy and AE count rate generated during the failure of LeiZhou fine granite. So, it can be concluded that the plagioclase content and grain size may be the main reasons for the different AE characteristics in rock failure.

Additionally, the Mohs hardness ranking proposed by Friedrich Mohs, a German mineralogist in 1822, the hardness of quartz is 7 and feldspar is 6–6.5. Although the sedimentary rocks contain a large amount of quartz, its strength and energy generated during the failure are not as large as those generated by igneous rocks. This phenomenon explains that the influence of mineral hardness on rock strength seems not to be the main factor, and the influence

Table 8 AE count rate and cumulative AE count rate, AE hit rate, and cumulative AE hit rate, energy, and cumulative energy of the test rocks

Rock no.	Test type	AE count rate	Cumulative AE count rate	AE hit rate	Cumulative AE hit rate	Energy (mV*ms)	Cumulative energy (mV*ms)
1	UCT	13,648	495,492	1040	97,389	28,213	803,771
	BIT	45,447	176,032	998	16,837	16,462	84,199
2	UCT	57,883	73,622	852	3561	4325	14,162
	BIT	22,524	87,944	768	10,282	17,160	56,120
3	UCT	143,777	589,055	1058	11,584	25,188	213,538
	BIT	55,909	240,533	993	17,062	9311	69,761
4	UCT	2855	1,019,759	908	516,076	570	709,179
	BIT	2794	29,227	689	23,654	294	55,893
5	UCT	1069	314,987	4233	608,573	107	406,067
	BIT	576	42,685	923	45,832	4460	5948
6	UCT	325	40,022	3675	56,824	633	7365
	BIT	275	35,621	782	16,985	258	5396
7	UCT	14,556	202,759	1008	40,417	429	46,039
	BIT	2385	16,626	706	12,518	326	15,361
8	UCT	31,502	153,454	899	17,783	2074	39,202
	BIT	17,879	49,747	895	4034	8078	14,632
10	UCT	166,653	1,220,730	1059	41,729	65,535	530,313
	BIT	49,870	113,059	654	3444	65,652	106,322
11	UCT	206,296	3,118,760	1063	200,807	65,268	1,699,353
	BIT	19,894	163,092	812	9590	2744	43,724
12	UCT	257,803	4,974,004	893	29,163	65,745	2,189,545
	BIT	106,357	362,868	673	6837	30,030	114,952

of mineralogy and texture characteristics on rock strength is more important than hardness.

5 Conclusions

In this study, 13 different types of rock mineral composition and particle size statistics are presented and analyzed. At the same time, acoustic emission technology and the failure modes of six typical rocks under UCT and BIT were combined and classified. This study applies comparative analysis to investigate the relationship between AE hit rate, the AE count rate, and AE energy with the rock failure mode and texture characteristics. Secondly, the effects of different types of rock mineral composition content and mineral grain size on the basic mechanical properties were investigated. Finally, a simple regression analysis is described for the relationships between static (density, P -wave velocity V_p , Schmidt Hammer rebound hardness value (SHV)) and basic mechanical parameters (σ_c , σ_p , E) of the rock. The results are as follows:

1. When the data set in the AF–RA nuclear density map is close to the AF axis with a long side, and lower than 100 or the AE peak frequency distribution is between 200 and 400 kHz, the rock is mainly caused by tensile failure. When the data set is near the RA axis with a long side or the AE peak frequency distribution is below 100, the rock mainly fails due to shear. These results provide a method to distinguish the main failure modes of rock by acoustic emission technology, which facilitates the identification and detection of practical engineering problems.
2. The peak value of the AE hit rate generated by igneous rocks is usually about 101 times higher than the weak rocks. Moreover, the AE signals characteristics mainly depend on the rock lithology difference and have little correlation with the failure mode. The cumulative AE count rate and cumulative energy are positively correlated with the increase of plagioclase content, but as the quartz content increases, the cumulative AE count rate decreases and the cumulative energy first decreases and then increases. With the increase of K-feldspar content, the cumulative AE count rate and cumulative energy

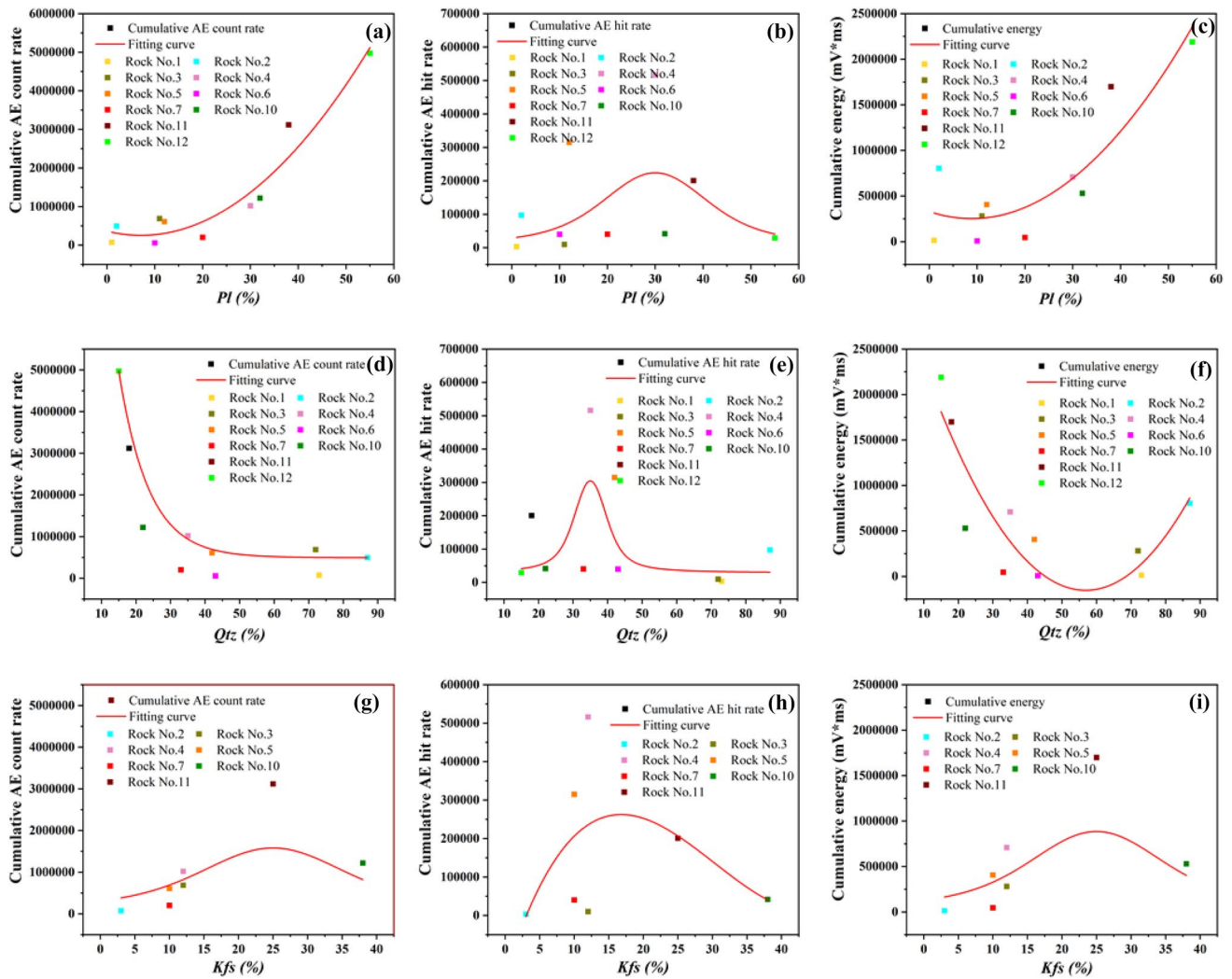


Fig. 22 Relationship between mineral composition content and AE characteristics in UCT: a–c plagioclase; d–f quartz; g–i k-feldspar

first increase and then decreases. In addition, the results show that the cumulative energy generated by the rock failure with larger grain sizes is larger than the rocks with smaller particle sizes.

- For different rock mineral compositions on the impact of rock strength, igneous rock strength is positively correlated with plagioclase content, and negatively correlated with quartz and K-feldspar. The sedimentary rock strength first increases and then decreases with the increase of plagioclase content, and decreases with the increase of quartz content, which has little correlation with the K-feldspar content. Plagioclase has a positive effect on rock strength. The mineral particle size rich-

ness may have a positive effect on the rock strength. Moreover, it is found that rock strength is inversely proportional to mineral particle size for igneous rocks. The experimental results provide a basis to predict the basic mechanical rock parameters using the mineral composition and grain size of the rocks.

- The rock static parameters (density, P -wave velocity V_p , Schmidt hammer rebound hardness value (SHV)), and basic mechanical parameters (σ_c , σ_p , E) were analyzed by simple regression analysis. It was found that the basic mechanical parameters are positively correlated with the static parameters. It provides theoretical support to predict rock strength with the static parameters of rock.

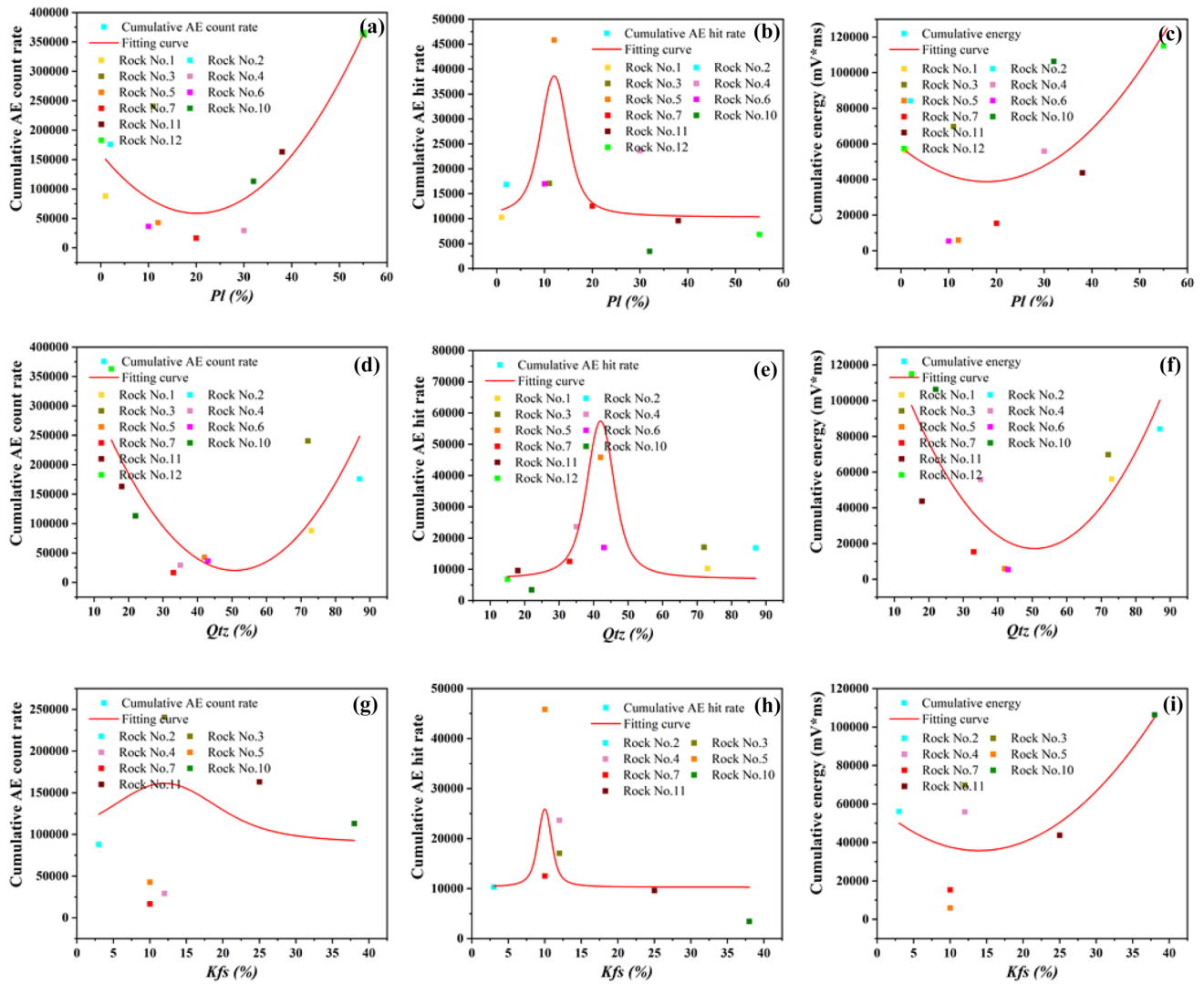
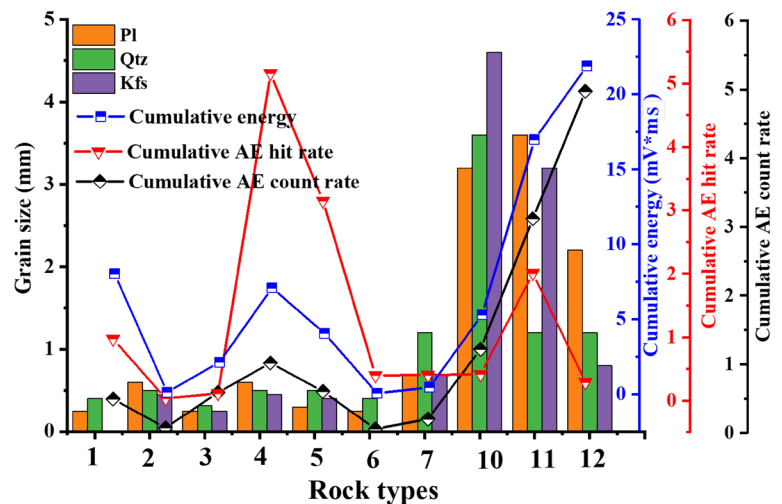


Fig. 23 Relationship between mineral composition content and AE characteristics in BIT: **a–c** plagioclase; **d–f** quartz; **g–i** k-feldspar

Fig. 24 Size of main mineral components with AE characteristics: (1) Rock No. 1, (2) Rock No. 2, (3) Rock No. 3, (4) Rock No. 4, (5) Rock No. 5, (6) Rock No. 6, (7) Rock No. 7, (8) Rock No. 10, (9) Rock No. 11, (10) Rock No. 12



Acknowledgements This research is partially supported by the science and technology innovation program of Hunan province (2021RC3007), the National Natural Science Foundation Project of China (42177164), the Distinguished Youth Science Foundation of Hunan Province of China (2022JJ10073) and the Innovation-Driven Project of Central South University (2020CX040).

Funding Open Access funding enabled and organized by CAUL and its Member Institutions.

Open Access This article is licensed under a Creative Commons Attribution 4.0 International License, which permits use, sharing, adaptation, distribution and reproduction in any medium or format, as long as you give appropriate credit to the original author(s) and the source, provide a link to the Creative Commons licence, and indicate if changes were made. The images or other third party material in this article are included in the article's Creative Commons licence, unless indicated otherwise in a credit line to the material. If material is not included in the article's Creative Commons licence and your intended use is not permitted by statutory regulation or exceeds the permitted use, you will need to obtain permission directly from the copyright holder. To view a copy of this licence, visit <http://creativecommons.org/licenses/by/4.0/>.

References

- Baud P, Wong T-F, Zhu W (2014) Effects of porosity and crack density on the compressive strength of rocks. *Int J Rock Mech Min Sci* 67:202–211. <https://doi.org/10.1016/j.ijrmms.2013.08.031>
- Brace WF (1961) Dependence of fracture strength of rocks on grain size. In: The 4th US Symposium on Rock Mechanics (USRMS)
- Dong LJ, Chen YC, Sun DY, Zhang YH (2021) Implications for rock instability precursors and principal stress direction from rock acoustic experiments. *Int J Min Sci Technol* 31:789–798
- Du K, Tao M, Li XB, Zhou J (2016) Experimental study of slabbing and rockburst induced by true-triaxial unloading and local dynamic disturbance. *Rock Mech Rock Eng* 49(9):3437–3453
- Du K, Su R, Tao M, Yang CZ, Momeni A, Wang SF (2019) Specimen shape and cross-section effects on the mechanical properties of rocks under uniaxial compressive stress. *Bull Eng Geol Env* 78:6061–6074
- Du K, Li X-F, Yang C-Z, Jian Z, Shao JC, Khandelwal M (2020a) Experimental investigations into the mechanical performance of marble and sandstone under biaxial confinements. *J Central South Univ* 27(10):2985–2998
- Du K, Li X, Tao M, Wang S (2020b) Experimental study on acoustic emission (AE) characteristics and crack classification during rock fracture in several basic lab tests. *Int J Rock Mech Min Sci* 133:104411
- Du K, Yang C, Su R, Tao M, Wang S (2020c) Failure properties of cubic granite, marble, and sandstone specimens under true triaxial stress. *Int J Rock Mech Mining Sci* 130:104309
- Du K, Sun Y, Zhou J, Wang SF, Tao M, Yang C, Khandelwal M (2021) Low amplitude fatigue performance of sandstone, marble, and granite under high static stress. *Geomech Geophys Geo-Energy Geo-Resour* 7(3):1–21
- Du K, Li XF, Su R, Tao M, Lv SZ, Luo J, Zhou J (2022) Shape ratio effects on the mechanical characteristics of rectangular prism rocks and isolated pillars under uniaxial compression. *Int J Min Sci Technol* 32(2):347–362
- Dunn DE, LaFountain LJ, Jackson RE (1973) Porosity dependence and mechanism of brittle fracture in sandstones. *J Geophys Res* 78:2403–2417
- Gunsallus KL, Kulhawy FH (1984) A comparative evaluation of rock-strength measures. *Int J Rock Mech Min Sci* 21:233–248
- Gupta AS, Rao KS (2000) Weathering effects on the strength and deformational behaviour of crystalline rocks under uniaxial compression state. *Eng Geol* 56:257–274
- Gutenberg B, Richter CF (1944) Frequency of earthquakes in California. *Bull Seismol Soc Am* 34(4):185–188
- Handin J, Hager RV (1957) Experimental deformation of sedimentary rocks under confining pressure: tests at room temperature on dry samples. *AAPG Bull* 41:1–50
- Hecht CA, Bönsch C, Bauch E (2005) Relations of rock structure and composition to petrophysical and geomechanical rock properties: examples from perm carboniferous red-beds. *Rock Mech Rock Eng* 38:197–216
- Irfan TY (1996) Mineralogy, fabric properties and classification of weathered granites in Hong Kong. 29:5–35
- Irfan TY, Dearman WR (1978) Engineering classification and index properties of a weathered granite. *Bull Int Assoc Eng Geol* 17:79–90
- KH (1974) Effect of porosity on the strength of the clastic sedimentary rocks. *Int J Rock Mech Min Sci Geomech Abstr* 13:25
- Khandelwal M, Ranjith PG (2017) Study of crack propagation in concrete under multiple loading rates by acoustic emission. *Geomech. Geophys. Geo-Energy Geo-Resour* 3(4):393–404. <https://doi.org/10.1007/s40948-017-0067-1>
- Kusunose K, Lei X, Nishizawa O, Satoh T (1991) Effect of grain size on fractal structure of acoustic emission hypocenter distribution in granitic rock. *Phys Earth Planet Interior* 67:194–199
- Li L, Aubertin M (2003) A general relationship between porosity and uniaxial strength of engineering materials. *Revue Canadienne De Génie Civil* 30(4):644–658
- Lindqvist JE, Åkesson U, Malaga K (2007) Microstructure and functional properties of rock materials. *Mater Charact* 58(11–12):1183–1188
- Liu PF, Zhou XP, Qian Q (2021) Experimental investigation of rigid confinement effects of radial strain on dynamic mechanical properties and failure modes of concrete. *Int J Min Sci Technol* 31(05):939–951
- Lokajicek T, Vlk J (1996) Complex multichannel system for continuous monitoring of AE and related parameters. In: Rogers LM, Tscheliesnig P (eds) *Proc 22nd European Conference on Acoustic Emission Testing*, The Robert Gordon University, Aberdeen, UK, pp 271–275
- Ministry of Land and Resources, PRC (2015) Technical specification for rock and ore identification—part 4: Identification of thin sections of rock: DZ/T 0275.4-2015[S]
- Moradian Z, Einstein HH, Ballivy G (2016) Detection of cracking levels in brittle rocks by parametric analysis of the acoustic emission signals. *Rock Mech Rock Eng* 49(3):785–800
- Novikov EA, Oshkin RO, Shkuratnik VL, Epshtein SA, Dobryakova NN (2018) Application of thermally stimulated acoustic emission method to assess the thermal resistance and related properties of coals. *Int J Min Sci Technol* 28(2):243–249
- Olsson WA (1974) Grain size dependence of yield stress in marble. *J Geophys Res* 79:4859–4862
- Onodera TF, Kumara HMA (1980) Relation between texture and mechanical properties of crystalline rocks
- Ozcelik Y, Bayram F, Yasitli NE (2013) Prediction of engineering properties of rocks from microscopic data. *Arab J Geosci* 6:3651–3668
- Pikryl R (2001) Some microstructural aspects of strength variation in rocks. *Int J Rock Mech Min Sci* 38:671–682
- Přikryl R, Lokajček T, Li C, Rudajev V (2003) Acoustic emission characteristics and failure of uniaxially stressed granitic rocks: the effect of rock fabric. *Rock Mech Rock Eng* 36(4):255–270

- Rao MVMS, Lakshmi KJP (2005) Analysis of b-value and improved b-value of acoustic emissions accompanying rock fracture. *Curr Sci* 89(9):1577–1582
- Richard M, Rieke HH, Kim YC (1970) Tensile strength related to mineralogy and texture of some granitic rocks. *Eng Geol* 4:155–160
- Rui YC, Zhou ZL, Lu JY, Ullah B, Cai X (2022) A novel AE source localization method using clustering detection to eliminate abnormal arrivals. *Int J Min Sci Technol* 32(01):51–62
- Shakoor A, Bonelli RE (1991) Relationship between petrographic characteristics, engineering index properties, and mechanical properties of selected sandstones. *Int J Rock Mech Min Sci Geomech Abstr* 28:55–71
- Tao ZA, Ly A, Hs A, Qiang ZA, Sc B (2021) Experimental and numerical investigations on the tensile mechanical behavior of marbles containing dynamic damage. *Int J Min Sci Technol*
- Torabi-Kaveh M, Naseri F, Saneie S, Sarshari B (2015) Application of artificial neural networks and multivariate statistics to predict UCS and E using physical properties of Asmari limestones. *Arab J Geosci* 8:2889–2897
- Tuğrul A, Zarif IH (1999) Correlation of mineralogical and textural characteristics with engineering properties of selected granitic rocks from Turkey. *Eng Geol* 51(4):303–317. [https://doi.org/10.1016/S0013-7952\(98\)00071-4](https://doi.org/10.1016/S0013-7952(98)00071-4).
- Ulusay R, Türeli K, Ider MH (1994) Prediction of engineering properties of a selected litharenite sandstone from its petrographic characteristics using correlation and multivariate statistical techniques. *Eng Geol* 38:135–157
- Wang H, Liu D, Cui Z, Cheng C, Jian Z (2016) Investigation of the fracture modes of red sandstone using XFEM and acoustic emissions. *Theor Appl Fract Mech* 85:283–293
- Wang S, Liu Y, Du K, Zhou J, Khandelwal M (2020) Waveform features and failure patterns of hollow cylindrical sandstone specimens under repetitive impact and triaxial confinements. *Geomech. Geophys. Geo-Energy Geo-Resour.* 6(4):1–18
- Wang SM, Zhou J, Li CQ, Armaghani DJ, Li XB, Mitri HS (2021) Rockburst prediction in hard rock mines developing bagging and boosting tree-based ensemble techniques. *J Cent South Univ* 28(2):527–542
- Wen T, Zhang X, Sun JS, Jia YS, Lang M, Jia WJ, Li DC, Sun LX, Tang HM (2021) Evaluation of rock brittleness based on pre-peak and post-peak energy evolution characteristics. *Earth Sci* 46(09):3385–3396
- Wong Robina HC, Chau KT, Wang P (1996) Microcracking and grain size effect in Yuen Long marbles. *Int J Rock Mech Min Sci Geomech Abstr* 33:479–485
- Xue DJ, Zhang ZP, Chen C, Zhou J, Lu L, Sun XT, Liu YT (2021) Spatial correlation-based characterization of acoustic emission signal-cloud in a granite sample by a cube clustering approach. *Int J Min Sci Technol* 31(04):535–551
- Zhen H, Qi XG, Yu FW, Yun W, Shi JL, Kui Z, Rui Z (2021) Effects of confining pressure on acoustic emission and failure characteristics of sandstone. *Int J Min Sci Technol* 05:963–974
- Zhou J, Li X, Mitri HS (2018) Evaluation method of rockburst: state-of-the-art literature review. *Tunnel Underground Space Technol* 81:632–659
- Zhou J, Chen C, Du K, Jahed Armaghani D, Li C (2022a) A new hybrid model of information entropy and unascertained measurement with different membership functions for evaluating destressability in burst-prone underground mines. *Eng Comput* 38:381–399
- Zhou J, Chen C, Wei C, Du K (2022b) An improved connection cloud model of an updated database: a multicriteria uncertainty model for coal burst liability evaluation. *Nat Res Res* 31(3):1687–1704

Publisher's Note Springer Nature remains neutral with regard to jurisdictional claims in published maps and institutional affiliations.